Lawrence Berkeley Laboratory
UNIVERSITY OF CALIFORNIA

Materials & Chemical Sciences Division

To be published as a chapter in **Modern Superconducting Devices**, S.T. Ruggiero and D.A. Rudman, Eds., Academic Press, Inc., Orlando, FL

SQUIDS: Principles, Noise, and Applications

J. Clarke

November 1988

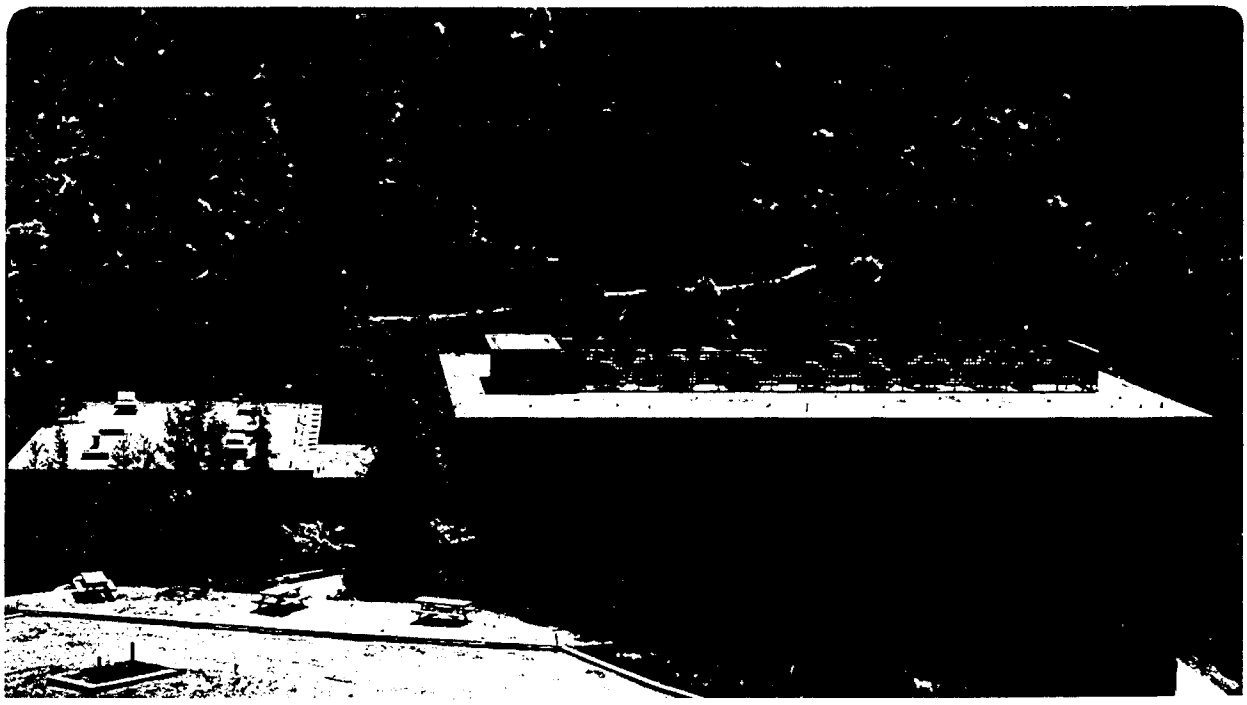

Prepared for the U.S. Department of Energy under Contract Number DE-AC03-76SF00098.

DISCLAIMER

SQUIDS: PRINCIPLES, NOISE AND APPLICATIONS

John Clarke

Department of Physics, University of California
and
Materials and Chemical Sciences Division, Lawrence Berkeley Laboratory
One Cyclotron Road, Berkeley, California 94720

This chapter is a shortened version of a chapter in the proceedings of the NATO Advanced Study Institute on Superconductive Electronics, edited by M. Nisenoff and H. Weinstock.

TABLE OF CONTENTS

1. INTRODUCTION

Superconducting QUantum Interference Devices (SQUIDs) are the most sensitive detectors of magnetic flux available. A SQUID is, in essence, a flux-to-voltage transducer, providing an output voltage that is periodic in the applied flux with a period of one flux quantum, $\Phi_0 \equiv h/2e \approx 2.07 \times 10^{-15}$ Wb. One is generally able to detect an output signal corresponding to a flux change of much less than Φ_0. SQUIDs are amazingly versatile, being able to measure any physical quantity that can be converted to a flux, for example, magnetic field, magnetic field gradient, current, voltage, displacement, and magnetic susceptibility. As a result, their applications are wide ranging, from the detection of tiny magnetic fields produced by the human brain and the measurement of fluctuating magnetic fields in remote areas to the detection of gravity waves and the observation of spin noise in an ensemble of magnetic nuclei.

SQUIDs combine two physical phenomena, flux quantization -- the fact that the flux Φ in a closed superconducting loop is quantized[1] in units of Φ_0 -- and Josephson tunneling [2]. There are two kinds of SQUIDs. The first[3], the dc SQUID, consists of two Josephson junctions connected in parallel on a superconducting loop, and is so named because it operates with a steady current bias. Relatively crude devices were developed in the second half of the 1960's, and used successfully by low temperature physicists to measure a variety of phenomena occurring at liquid helium temperatures. At the end of the decade, the rf SQUID [4,5] appeared. This device involves a single Josephson junction interrupting the current flow around a superconducting loop, and is operated with a radiofrequency flux bias.

Because it required only a single junction, at the time the rf SQUID was simpler to manufacture and quickly became commercially available. It has remained the more widely used device ever since. However, in the mid-1970's, it was shown that the dc SQUID was the more sensitive device, and there has been an ongoing development of thin-film dc SQUIDs and instruments based on them since then. By contrast, there has been little development of the rf SQUID in the last decade.

In this chapter I give an overview of the current state of the SQUID art; I cannot hope to describe all of the SQUIDs that have been made or, even less, all of the applications in which they have been successfully used. I begin, in Section 2, with a brief review of the resistively shunted Josephson junction, with particular emphasis on the effects of noise. Section 3 contains a description of the dc SQUID -- how these devices are made and operated, and the limitations imposed by noise. Section 4 contains a similar description of the properties of rf SQUIDs, but because there has been little development of these devices in the 1980's I shall keep this section relatively brief. In Section 5, I describe a selection of instruments based on SQUIDs and mention some of their applications. Section 6 is a discussion of the impact of high temperature superconductivity on SQUIDs, and of future prospects in this area, and Section 7 contains a few concluding remarks.

2. THE RESISTIVELY SHUNTED JUNCTION

The Josephson junction[2] consists of two superconductors separated by a thin insulating barrier. Cooper pairs of electrons (or holes) are able to tunnel through the barrier, maintaining phase coherence in the process. The applied

current, I, controls the difference $\delta = \phi_1 - \phi_2$ between the phases of the two superconductors according to the current-phase relation

$$I = I_0 \sin \delta, \tag{2.1}$$

where I_0 is the critical current, that is, the maximum supercurrent the junction can sustain. When the current is increased from zero, initially there is no voltage across the junction, but for $I > I_0$ a voltage V appears and δ evolves with time according to the voltage frequency relation

$$\dot{\delta} = 2eV/\hbar = 2\pi V/\Phi_0. \tag{2.2}$$

A high quality Josephson tunnel junction has a hysteretic current -voltage (I-V) characteristic. As the current is increased from zero, the voltage switches abruptly to a nonzero value when I approaches I_0, but returns to zero only when I is reduced to a value much less than I_0. This hysteresis must be eliminated for SQUIDs operated in the conventional manner, and one does so by shunting the junction with an external shunt resistance. The "resistively shunted junction" (RSJ) model [6,7] is shown in Fig.1(a). The junction has a critical current I_0 and is in parallel with its self-capacitance C and the shunt resistance R, which has a current noise source $I_N(t)$ associated with it. The equation of motion is

$$C\dot{V} + I_0 \sin \delta + V/R = I + I_N(t). \tag{2.3}$$

Neglecting the noise term for the moment and setting $V = \hbar\dot{\delta}/2e$, we obtain

$$\frac{\hbar C}{2e}\ddot{\delta} + \frac{\hbar}{2eR}\dot{\delta} = I - I_0 \sin \delta = -\frac{2e}{\hbar}\frac{\partial U}{\partial \delta}, \tag{2.4}$$

where

$$U = -\frac{\Phi_0}{2\pi}(I\delta + I_0 \cos\delta). \qquad (2.5)$$

One obtains considerable insight into the dynamics of the junction by realizing that Eq. (2.4) also describes the motion of a ball moving on the "tilted washboard" potential U. The term involving C represents the mass of the particle and 1/R the damping of the motion; the average "tilt" of the washboard is proportional to -I. For values of $I<I_0$, the particle is confined to one of the potential wells [Fig. 1(b)], where it oscillates back and forth at the plasma frequency[1] $\omega_p = (2\pi I_0/\Phi_0 C)^{1/2} [1 - (I/I_0)^2]^{1/4}$; in this state $<\dot{\delta}>$ and hence the average voltage across the junction are zero (< > represents a time average). When the current is increased to I_0, the tilt increases so that the particle rolls down the washboard; in this state $<\delta>$ is nonzero and a voltage appears across the junction [Fig. 1(c)]. As the current is increased further, $<\dot{\delta}>$ increases, as does V. For the nonhysteretic case, as soon as I is reduced below I_0 the particle becomes trapped in one of the wells, and V returns to zero. In this, the overdamped case, we require[6,7]

$$\beta_C \equiv (2\pi I_0 R/\Phi_0)RC = \omega_J RC \lesssim 1; \qquad (2.6)$$

$\omega_J / 2\pi$ is the Josephson frequency corresponding to the voltage $I_0 R$.

We introduce the effects of noise by restoring the noise term to Eq. (2.4) to obtain the Langevin equation

$$\frac{\hbar C}{2e}\ddot{\delta} + \frac{\hbar}{2eR}\dot{\delta} + I_0 \sin\delta = I + I_N(t). \qquad (2.7)$$

In the thermal noise limit, the spectral density of $I_N(t)$ is given by the Nyquist formula

$$S_I(\nu) = 4k_B T / R, \qquad (2.8)$$

where ν is the frequency. It is evident that $I_N(t)$ causes the tilt in the washboard to fluctuate with time. This fluctuation has two effects on the junction. First, when I is less than I_0, from time to time fluctuations cause the total current $I + I_N(t)$ to exceed I_0, enabling the particle to roll out of one potential minimum into the next. For the underdamped junction, this process produces a series of voltage pulses randomly spaced in time. Thus, the time average of the voltage is nonzero even though $I < I_0$, and the I - V characteristic is "noise-rounded" at low voltages.[8] Because this thermal activation process reduces the observed value of the critical current, there is a minimum value of I_0 for which the two sides of the junction remain coupled together. This condition may be written as

$$I_0\Phi_0/2\pi \gtrsim 5k_B T, \qquad (2.9)$$

where $I_0\Phi_0 / 2\pi$ is the coupling energy of the junction[2] and the factor of 5 is the result of a computer simulation[9]. For T = 4.2K, we find $I_0 \gtrsim 0.9\mu A$.

The second consequence of thermal fluctuations is voltage noise. In the limit $\beta_C << 1$ and for $I > I_0$, the spectral density of this noise at a measurement frequency ν_m that we assume to be much less than the Josephson frequency ν_J is given by[10,11]

$$S_V(\nu_m) = \left[1+\frac{1}{2}\left(\frac{I_0}{I}\right)^2\right] \frac{4k_BTR_d^2}{R} \cdot \left\{ \begin{array}{c} \beta_C << 1 \\ I > I_0 \\ \nu_m << \nu_J \end{array} \right\} \quad (2.10)$$

The first term on the right-hand side of Eq. (2.10) represents the Nyquist noise current generated at the measurement frequency ν_m flowing through the dynamic resistance $R_d \equiv dV/dI$ to produce a voltage noise. The second term, $(1/2)(I_0 / I)^2 \times (4k_BT/R)\, R_d^2$, represents Nyquist noise generated at frequencies $\nu_J \pm \nu_m$ mixed down to the measurement frequency by the Josephson oscillations and the inherent nonlinearity of the junction. The factor $(1/2)(I_0 / I)^2$ is the mixing coefficient, and it vanishes for sufficiently large bias currents. The mixing coefficients for the Nyquist noise generated near harmonics of the Josephson frequencies, $2\nu_J$, $3\nu_J$, ---, are negligible in the limit $\nu_m / \nu_J << 1$.

At sufficiently high bias current the Josephson frequency ν_J exceeds k_BT/h, and quantum corrections[12] to Eq. (2.10) become important provided the term $(1/2)(I_0 / I)^2$ is not too small. It turns out that the requirement for observing significant quantum corrections is $eI_0R / k_BT >> 1$. The spectral density of the voltage noise becomes

$$S_V(\nu_m) = \left[\frac{4k_BT}{R} + \frac{2eV}{R}\left(\frac{I_0}{I}\right)^2 \coth\left(\frac{eV}{k_BT}\right)\right] R_d^2, \quad \left\{ \begin{array}{c} \beta_C << 1 \\ I > I_0 \\ \nu_m << \nu_J \end{array} \right\} \quad (2.11)$$

where we have assumed that $h\nu_m / k_BT << 1$ so that the first term on the right-hand side of Eq. (2.11) remains in the thermal limit. In the limit $T \rightarrow 0$, the second term, $(2eV/R)\,(I_0 / I)^2 R_d^2$, represents noise mixed down from zero point fluctuations near the Josephson frequency.

This concludes our review of the RSJ, and we now turn our attention to the dc SQUID.

3. THE DC SQUID

3.1 Theory of Operation

The essence of the dc SQUID[3] is shown in Fig. 2(a). Two Josephson junctions are connected in parallel on a superconducting loop of inductance L. Each junction is resistively shunted[6,7] to eliminate hysteresis on the current-voltage (I -V) characteristics, which are shown in Fig.2(b) for $\Phi = n\Phi_0$ and $(n + 1/2)\Phi_0$; Φ is the external flux applied to the loop and n is an integer. If we bias the SQUID with a constant current ($> 2\, I_0$), the voltage across the SQUID oscillates as we steadily increase Φ, as indicated in Fig. 2(c). The period is Φ_0 . The SQUID is generally operated on the steep part of the V - Φ curve where the transfer coefficient, $V_\Phi \equiv | (\partial V/\partial \Phi)_I |$, is a maximum. Thus, the SQUID produces an output voltage in response to a small input flux $\delta\Phi$ ($<< \Phi_0$), and is effectively a flux-to-voltage transducer. The resolution can be characterized by the equivalent flux noise, Φ_N (t), which has a spectral density

$$S_\Phi(f) = S_V(f)/ V_\Phi^2 \qquad (3.1)$$

at frequency f. Here, $S_V(f)$ is the spectral density of the voltage noise across the SQUID at fixed current bias. A more useful characterization, however, is in terms of the flux noise energy associated with $S_\Phi(f)$,

$$\varepsilon(f) = S_\Phi(f) / 2L, \qquad (3.2)$$

where L is the inductance of the loop.

Thermal noise imposes two constraints on the parameters of the SQUID. First, the coupling energy, $I_0\Phi_0/2\pi$, of each junction must be significantly greater than k_BT; a computer analysis yields[9].

$$I_0\Phi_0/2\pi \gtrsim 5k_BT. \tag{3.3}$$

At 4.2K, Eq. (2.3) implies $I_0 \gtrsim 0.9\mu A$. Second, the root mean square thermal noise flux in the loop, $\langle\Phi_N^2\rangle^{1/2} = (k_BTL)^{1/2}$, must be significantly less than Φ_0; the same computer analysis[9] leads to

$$L \lesssim \Phi_0^2/5k_BT. \tag{3.4}$$

This constraint implies $L \lesssim 15nH$ at 4.2K.

We now outline the signal and noise properties of the SQUID. Each junction in Fig. 2(a) has a critical current I_O, a self-capacitance C and a resistive shunt R chosen so that $\beta_c \equiv 2\pi I_0R^2C/\Phi_0 \lesssim 1$. The two resistors generate statistically independent Nyquist noise currents, $I_{N1}(t)$ and $I_{N2}(t)$, each with a spectral density $4k_BT/R$ at temperature T. The differences in the phase across each junction, $\delta_1(t)$ and $\delta_2(t)$, obey the following equations[13-15]:

$$V = \frac{\hbar}{4e}\left(\dot{\delta}_1 + \dot{\delta}_2\right), \tag{3.5}$$

$$J = \frac{\Phi_0}{2\pi L}\left(\delta_1 - \delta_2 - \frac{2\pi\Phi}{\Phi_0}\right), \tag{3.6}$$

$$\frac{\hbar C}{2e}\ddot{\delta}_1 + \frac{\hbar}{2eR}\dot{\delta}_1 = \frac{I}{2} - J - I_0 \sin\delta_1 + I_{N1}, \tag{3.7}$$

and

$$\frac{\hbar C}{2e}\ \ddot{\delta}_2 + \frac{\hbar}{2eR}\ \dot{\delta}_2 = \frac{I}{2} + J - I_0 \sin \delta_2 + I_{N_2}\,. \qquad (3.8)$$

Equation (3.5) relates the voltage to the average rate of change of phase, Eq. (3.6) expresses fluxoid quantization, and Eqs. (3.7) and (3.8) are Langevin equations coupled via J. These equations have been solved numerically for a limited range of values of the noise parameter $\Gamma = 2\pi k_B T/I_0\Phi_0$, reduced inductance $\beta = 2\,LI_0 / \Phi_0$ and hysteresis parameter β_C. For typical SQUIDs in the ^{4}He temperature range, $\Gamma = 0.05$. One computes the time averaged voltage V vs. Φ, and hence finds V_Φ, which, for a given value of Φ, peaks smoothly as a function of bias current. The transfer function exhibits a shallow maximum around $(2n + 1)\,\Phi_0 / 4$. One computes the noise voltage for a given value of Φ as a function of I, and finds that the spectral density is white at frequencies much less than the Josephson frequency. For each value of Φ, the noise voltage peaks smoothly at the value of I where V_Φ is a maximum. From these simulations, one finds that the noise energy has a minimum when $\beta \approx 1$. For $\beta = 1$, $\Gamma = 0.05$, $\Phi = (2n + 1)\,\Phi_0 / 4$ and for the value of I at which V_Φ is a maximum, the results can be summarized as follows:

$$V_\Phi \approx R/L, \qquad (3.9)$$

$$S_V(f) \approx 16 k_B T R, \qquad (3.10)$$

and

$$\varepsilon(f) \approx 9 k_B T L/R. \qquad (3.11)$$

It is often convenient to eliminate R from Eq. (3.11) using the expression $R = (\beta_C\,\Phi_0 / 2\pi I_0 C)^{1/2}$. We find

$$\varepsilon(f) \approx 16\, k_B T (LC/\beta_C)^{1/2}. \quad (\beta_C \lesssim 1) \qquad (3.12)$$

Equation (3.12) gives a clear prescription for improving the resolution: one should reduce T, L and C. A large number of SQUIDs with a wide range of parameters have been tested, and found to have noise energies generally in good agreement with the predicted values. It is common practice to quote the noise energy of SQUIDs in units of $\hbar$ ($\approx 10^{-34}$J sec = 10^{-34}JHz^{-1}).

3.2 Practical dc SQUIDs

Modern dc SQUIDs are invariably made from thin films, with the aid of either photolithography or electron beam lithography. A major concern in the design is the need to couple an input coil inductively to the SQUID with rather high efficiency. This problem was elegantly solved by Ketchen and Jaycox,[16,17] who introduced the idea of depositing a spiral input coil on a SQUID in a square washer configuration. The coil is separated from the SQUID with an insulating layer. The version[18] of this design made at UC Berkeley is shown in Fig. 3. These devices are made in batches of 36 on 50mm diameter oxidized silicon wafers in the following way. First, a 30nm thick Au (25 wt % Cu) film is deposited and patterned to form the resistive shunts. Next, we sputter a 100nm thick Nb film and etch it to form the SQUID loop and a strip that eventually contacts the inner end of the spiral coil. The third film is a 200nm SiO layer with 2μm diameter windows for the junctions, a larger window to give access to the CuAu shunt, and a window at each end of the Nb strip to provide connections to the spiral coil. The next step is to deposit and lift-off the 300nm thick Nb spiral coil, which has 4, 20 or 50 turns. At this point, we usually dice the wafer into chips, each with a single SQUID which is completed individually. The device is ion-milled to clean the exposed areas of Nb and CuAu. We have two procedures for forming the oxide barrier. In one, we oxidize the Nb in a rf discharge in Ar

containing 5 vol % O_2, and deposit the 300nm Pb (5wt % In) counterelectrode which completes the junctions and makes contact with the shunts. In the other process, we deposit approximately 6nm of Al and form Al_2O_3 by exposing[19] it to O_2. A photograph of the completed SQUID and a scanning electron micrograph of the junctions is shown in Fig. 4. The shunt resistance R is typically 8Ω, and the estimated capacitance C about 0.5pF.

Jaycox and Ketchen[17] showed that a square washer (with no slit) with inner and outer edges d and w has an inductance L (loop) = $1.25\mu_0 d$ in the limit w >>d. They gave the following expressions for the inductances of the SQUID, L, and of the spiral coil, L_i, and for the mutual inductance, M_i, and coupling coefficient, α^2, between the spiral coil and the SQUID:

$$L = L\,(\text{loop}) + L_j, \tag{3.13}$$

$$L_i = n^2\,(L-L_j) + L_s, \tag{3.14}$$

$$M_i = n(L-L_j) \tag{3.15}$$

and

$$\alpha^2 = (1-L_J/L)/\,[1+L_s n^2(L-L_j)]. \tag{3.16}$$

Here, L_j is the parasitic inductance associated with the junctions, n is the number of turns on the input coil and L_s is the stripline inductance of this coil. For the SQUID just described with a 50 turn input coil one measures $L_i \approx 800$ nH, $M_i \approx$ 16 nH and $\alpha^2 \approx 0.75$. These results are in good agreement with the predictions if one takes the predicted value L(loop) ≈ 0.31 nH and assumes $L_j \approx 0.09$ nH to give L ≈ 0.4 nH. The stripline inductance (~ 10 nH) is insignificant for a 50 turn coil.

References 20-25 are a selection of papers describing SQUIDs fabricated on the Ketchen-Jaycox design. Some of the devices involve edge junctions, in

which the counterelectrode is a strip making a tunneling contact to the base electrode only at the edge. This technique enables one to make junctions with a small area and thus a small self-capacitance without resorting to electron-beam lithography. However, stray capacitances are often critically important. As has been emphasized by a number of authors, parasitic capacitance between the square washer and the input coil can produce resonances that in turn induce structure on the I-V characteristics and give rise to excess noise. One way to reduce these effects is to lower the shunt resistance to increase the damping. An alternative approach is to couple the SQUID to the signal via an intermediary superconducting transformer[24], so that the number of turns on the SQUID washer and the parasitic capacitance are reduced. Knuutila et al.[25] successfully damped the resonances in the input coil by terminating the stripline with a matched resistor. An alternative coupling scheme has been adopted by Carelli and Foglietti[26], who fabricated thin-film SQUIDs with many loops in parallel. The loops are coupled to a thin-film input coil surrounding them.

3.3 Flux-locked Loop

In most, although not all, practical applications one uses the SQUID in a feedback circuit as a null-detector of magnetic flux[27]. One applies a modulating flux to the SQUID with a peak-to-peak amplitude $\Phi_0/2$ and a frequency f_m usually between 100 and 500 kHz, as indicated in Fig. 5. If the quasistatic flux in the SQUID is exactly $n\Phi_0$ the resulting voltage is a rectified version of the input signal, that is, it contains only the frequency $2f_m$ [Fig. 5(a)]. If this voltage is sent through a lock-in detector referenced to the fundamental frequency f_m, the output will be zero. On the other hand, if the quasistatic flux is $(n + 1/4)\Phi_0$, the voltage across the SQUID is at frequency f_m [Fig. 5(b)], and the output from the lock-in will be a maximum. Thus, as one increases the flux from $n\Phi_0$ to $(n + 1/4)\Phi_0$, the

output from the lock-in will increase steadily; if one reduces the flux from $n\Phi_0$ to $(n - 1/4)\Phi_0$, the output will increase in the negative direction [Fig. 5(c)].

The alternating voltage across the SQUID is coupled to a low-noise preamplifier, usually at room temperature, via either a cooled transformer[28] or a cooled LC series-resonant circuit[27]. The first presents an impedance N^2R_d to the preamplifier and the second an impedance Q^2R_d, where R_d is the dynamic resistance of the SQUID at the bias point, N is the turns-ratio of the transformer, and Q is the quality factor of the tank circuit. The value of N or Q is chosen to optimize the noise temperature of the preamplifier; with careful design, the noise from the amplifier can be appreciably less than that from the SQUID at 4.2K.

Figure 6 shows a typical flux-locked loop in which the SQUID is coupled to the preamplifier via a cooled transformer. An oscillator applies a modulating flux to the SQUID. After amplification, the signal from the SQUID is lock-in detected and sent through an integrating circuit. The smoothed output is connected to the modulation and feedback coil via a large series resistor, R_f. Thus, if one applies a flux $\delta\Phi$ to the SQUID, the feedback circuit will generate an opposing flux $-\delta\Phi$, and a voltage proportional to $\delta\Phi$ appears across R_f. This technique enables one to measure changes in flux ranging from much less than a single flux quantum to many flux quanta. The use of a modulating flux eliminates 1/f noise and drift in the bias current and preamplifier. Using a modulation frequency of 500kHz, a double transformer between the SQUID and the preamplifier, and a two-pole integrator, Wellstood et al.[18] achieved a dynamic range of $\pm 2 \times 10^7$ $Hz^{1/2}$ for signal frequencies up to 6kHz, a frequency response from 0 to 70 kHz (±3dB), and a maximum slew rate of $3 \times 10^6 \Phi_0$ sec^{-1}.

3.4 Thermal Noise in the dc SQUID: Experiment

One determines the spectral density of the equivalent flux noise in the SQUID by connecting a spectrum analyzer to the output of the flux-locked loop. A representative power spectrum[29] is shown in Fig. 7: above a 1/f noise region, the noise is white at frequencies up to the roll-off of the feedback circuit. In this particular example, with L = 200pH and R = 8Ω, the measured flux noise was $S_\Phi^{1/2}$ = $(1.9 \pm 0.1) \times 10^{-6}\Phi_0 Hz^{-1/2}$, in reasonable agreement with the predictions of Eqs. (3.9) and (3.10), $1.3 \times 10^{-6}\Phi_0 Hz^{-1/2}$. The corresponding flux noise energy was 4×10^{-32} JHz ≈ 400 ħ. Many groups have achieved noise energies that are comparable or, with lower values of L or C, somewhat better.

Rather recently, Wellstood et al.[30] have operated SQUIDs in a dilution refrigerator at temperatures T below 1K , using a second dc SQUID as a preamplifier. They found that the noise energy scaled rather accurately with T at temperatures down to about 150mK, below which the noise energy became nearly constant. This saturation was traced to heating in the resistive shunts which prevented them from cooling much below 150mK. This heating is actually a hot electron effect:[31,32] the bottleneck in the cooling process is the rate at which the electrons can transfer energy to the phonons which, in turn, transfer energy to the substrate. The temperature of the shunts was lowered by connecting each of them to a CuAu "cooling fin" of large volume. The hot electrons diffuse into the fins where they rapidly transfer energy to other electrons. Since the "reaction volume" is now greatly increased, the numbers of electrons and phonons interacting are also increased, and the electron gas is cooled more effectively. In this way, the effective electron temperature was reduced to about 50mK when the SQUID was at a bath temperature of 20mK, with a concomitant reduction in ε to about 5ħ . Very recently Ketchen et al.[33] have achieved a noise energy of about 3ħ at 0.3K in a SQUID with L = 100pH and C = 0.14pF.

3.5 1/f Noise in dc SQUIDs

The white noise in dc SQUIDs is well understood. However, some applications of SQUIDs, for example neuromagnetism, require good resolution at frequencies down to 0.1Hz or less and the level of the 1/f or "flicker" noise becomes very important.

There are at least two separate sources of 1/f noise in the dc SQUID[34]. The first arises from 1/f noise in the critical current of the Josephson junctions, and the mechanism for this process is reasonably well understood[35]. In the process of tunneling through the barrier, an electron becomes trapped for a while and is subsequently released. While the trap is occupied, there is a local change in the height of the tunnel barrier and hence in the critical current density of that region. As a result, the presence of a signal trap causes the critical current of the junction to switch randomly back and forth between two values, producing a random telegraph signal. If the mean time between pulses is τ, the spectral density of this process is a Lorentzian, scaling as $\tau/[1+(2\pi f\tau)^2]$. In general, there may be several traps in the junction, each with its own characteristic time τ_i. Provided the traps are statistically independent, the superposition of these Lorentzians yields a 1/f power spectrum[36,37].

The second source of 1/f noise in SQUIDs appears to arise from the motion of flux lines trapped in the body of the SQUID[34], and is less well understood than the critical current noise. This mechanism manifests itself as a flux noise; for all practical purposes the noise source behaves as if an external flux noise were applied to the SQUID. Thus, the spectral density of the 1/f flux noise scales as V_Φ^2, and, in particular, vanishes at $\Phi = (n \pm 1/2)\Phi_0$ where $V_\Phi = 0$. By contrast, critical current noise is still present when $V_\Phi = 0$, although its magnitude does depend on the applied flux.

The level of 1/f flux noise appears to depend strongly on the microstructure of the thin films. For example, SQUIDs fabricated at Berkeley with Nb loops sputtered under a particular set of conditions show 1/f flux noise levels of typically[34] $10^{-10}\ \Phi_0^2\,Hz^{-1}$ at 1Hz. On the other hand, SQUIDs with Pb loops in exactly the same geometry exhibit a 1/f noise level of about $2x10^{-12}\Phi_0^2 Hz^{-1}$ at 1Hz, arising from critical current fluctuations. Tesche et al.[38] reported a 1/f noise level in Nb-based SQUIDs of about $3x10^{-13}\Phi_0^2 Hz^{-1}$, but did not specify the origin of the noise. Foglietti et al.[39] found a critical current 1/f noise corresponding to $2x10^{-12}\Phi_0^2 Hz^{-1}$, also in Nb based devices. Thus, we conclude that the quality of the Nb films plays a significant role in the level of 1/f flux noise.

There is an important practical difference between the two sources of 1/f noise: critical current noise can be reduced by a suitable modulation scheme whereas flux noise cannot. Several schemes have been devised[34,39,40] that involve switching both the bias current and the flux bias, and reductions in the spectral density of the 1/f noise due to critical current fluctuations of at least one order of magnitude have been achieved.

3.6 Alternative Read-Out Schemes

Although the flux modulation method described in Sec. 3.3 has been used successfully for may years, alternative schemes have recently been developed. These efforts have been motivated, at least in part, by the need to simplify the electronics required for the multichannel systems used in neuromagnetism (see Sec. 5.1). Fujimaki and co-workers[41] and Drung and co-workers[42] have devised schemes in which the output from the SQUID is sensed digitally and fed back as an analog signal to the SQUID to flux-lock the loop. Fujimaki et al.[41] used Josephson digital circuitry to integrate their feedback system on the same chip as

the SQUID so that the flux-locked signal was available directly from the cryostat. The system of Drung and co-workers, however, is presently the more sensitive with a flux resolution of about $10^{-6}\Phi_0 Hz^{-1/2}$ in a 50pH SQUID. These workers were also able to reduce the l/f noise in the system using a modified version of the modulation scheme of Foglietti et al.[39] Although they need further development, cryogenic digital feedback schemes offer several advantages: they are compact, produce a digitized output for transmission to room temperature, offer wide flux-locked bandwidths, and need not add any noise to the intrinsic noise of the SQUID.

In yet another system, Mück and Heiden[43] have operated a dc SQUID with hysteretic junctions in a relaxation oscillator. The oscillation frequency depends on the flux in the SQUID, reaching a maximum at $(n+1/2)\Phi_0$ and a minimum at $n\Phi_0$. A typical frequency modulation is 100kHz at an operating frequency of 10MHz. This technique produces large voltages across the SQUID so that no matching network to the room temperature electronics is required. The room temperature electronics is simple and compact, and the resolution is about $10^{-5}\Phi_0 Hz^{-1/2}$ for a SQUID at 4.2K with an inductance estimated to be about 80pH.

4. THE RF SQUID

4.1 Principles of Operation

Although the rf SQUID is still the more widely used device because of its long-standing commercial availability, it has seen very little development in recent years. For this reason I will give a rather brief account of its principles and noise limitations, following rather closely descriptions in earlier reviews.[44,45]

The rf SQUID[4,5] shown in Fig.8 consists of a superconducting loop of inductance L interrupted by a single Josephson junction with critical current I_0 and a nonhysteretic current-voltage characteristic. Flux quantization[1] imposes the constraint

$$\delta + 2\pi\Phi_T/\Phi_0 = 2\pi n, \tag{4.1}$$

on the total flux Φ_T threading the loop. The phase difference δ across the junction determines the supercurrent

$$I_s = -I_0 \sin (2\pi\Phi_T/\Phi_0), \tag{4.2}$$

flowing in the ring. A quasistatic external flux Φ thus gives rise to a total flux

$$\Phi_T = \Phi - LI_0 \sin (2\pi\Phi/\Phi_0). \tag{4.3}$$

The variation of Φ_T with Φ is sketched in Fig.9(a) for the typical value $LI_0 = 1.25\ \Phi_0$. The regions with positive slope are stable, whereas those with negative slope are not. A "linearized" version of Fig.9(a) showing the path traced out by Φ and Φ_T is shown in Fig.9(b). Suppose we slowly increase Φ from zero. The total flux Φ_T increases less rapidly than Φ because the response flux $-LI_S$ opposes Φ. When I_S reaches I_0, at an applied flux Φ_C and a total flux Φ_{TC}, the junction switches momentarily into a nonzero voltage state and the SQUID jumps from the k=0 to the k=1 quantum state. If we subsequently reduce Φ from a value just above Φ_C, the SQUID remains in the k=1 state until $\Phi = \Phi_0 - \Phi_C$, at which point I_S again exceeds the critical current and the SQUID returns to the k=0 state. In the same way, if we lower Φ to below $-\Phi_C$ and then increase it, a second hysteresis loop will be traced out. We note that this hysteresis occurs provided $LI_0 > \Phi_0/2\pi$; most practical SQUIDs are operated in this regime. For $LI_0 \approx \Phi_0$, the energy ΔE

dissipated when one takes the flux around a single hysteresis loop is its area divided by L:

$$\Delta E \approx I_0 \Phi_0. \qquad (4.4)$$

We now consider the radio frequency (rf) operation of the device. The SQUID is inductively coupled to the coil of an LC-resonant circuit with a quality factor $Q = R_T/\omega_{rf}L_T$ via a mutual inductance $M=K(LL_T)^{1/2}$. Here, L_T, C_T, and R_T are the inductance, capacitance and (effective) parallel resistance of the tank circuit, and $\omega_{rf}/2\pi$ is its resonant frequency, typically 20 or 30 MHz. The tank circuit is excited at its resonant frequency by a current $I_{rf} \sin\omega_{rf}t$ which generates a current of amplitude $I_T=QI_{rf}$ in the inductor. The voltage V_T across the tank circuit is amplified with a preamplifier with a high input impedance. First consider the case $\Phi=0$. As we increase I_{rf} from zero, the peak rf flux applied to the loop is $MI_T = QMI_{rf}$ and V_T increases linearly with I_{rf}. The peak flux becomes equal to Φ_C when $I_T = \Phi_C/M$ or $I_{rf} = \Phi_C/ MQ$, at A in Fig.10. The corresponding peak rf voltage across the tank circuit is

$$V_T^{(n)} = \omega_{rf}L_T\Phi_C/M, \qquad (4.5)$$

where the superscript (n) indicates $\Phi = n\Phi_0$, in this case with n=0. At this point the SQUID makes a transition to <u>either</u> the k = +1 state or the k = -1 state. As the SQUID traverses the hysteresis loop, energy ΔE is extracted from the tank circuit. Because of this loss, the peak flux on the next half cycle is less than Φ_C, and no transition occurs. The tank circuit takes many cycles to recover sufficient energy to induce a further transition, which may be into either the k = +1 or -1 states. If we now increase I_{rf}, transitions are induced at the same values of I_T and

V_T but, because energy is supplied at a higher rate, the stored energy builds up more rapidly after each energy loss ΔE, and transitions occur more frequently. In the absence of thermal fluctuations, the "step" AB in Fig.10 is at constant voltage. At B, a transition is induced on each positive and negative rf peak, and a further increase in I_{rf} produces the "riser" BC. At C, transitions from the $k = \pm 1$ to $k = \pm 2$ states occur and a second step begins. As we continue to increase I_{rf}, we observe a series of steps and risers.

If we now apply an external flux $\Phi = \Phi_0/2$, the hysteresis loops in Fig.9(b) are shifted by $\Phi_0/2$. Thus, a transition occurs on the positive peak of the rf cycle at a flux $(\Phi_c - \Phi_0/2)$, whereas on the negative peak the required flux is $-(\Phi_c + \Phi_0/2)$. As a result, as we increase I_{rf} from zero we observe the first step at D in Fig.10 at

$$V_T^{(n+1/2)} = \omega_{rf} L_T (\Phi_C - \Phi_0/2)/M. \qquad (4.6)$$

As we increase I_{rf} from D to F, the SQUID traverses only one hysteresis loop, corresponding to the $k = 0$ to $k = +1$ transition at $(\Phi_c - \Phi_0/2)$. A further increase in I_{rf} produces the riser FG, and at G transitions at a peak rf flux $-(\Phi_C + \Phi_0/2)$ begin. In this way, we observe a series of steps and risers for $\Phi = \Phi_0/2$, interlocking those for $\Phi = 0$ (Fig.10). As we increase Φ from zero, the voltage at which the first step appears will drop to a minimum (D) at $\Phi_0/2$ and rise to its maximum value (A) at $\Phi = \Phi_0$. The change in V_T as we increase Φ from 0 to $\Phi_0/2$, found by subtracting Eq. (4.6) from Eq.(4.5), is $\omega_{rf} L_T \Phi_0/2M$. Thus, for a small change in flux near $\Phi = \Phi_0/4$ we find the transfer function

$$V_\Phi = \omega_{rf} L_T / M. \qquad (4.7)$$

At first sight, Eq.(4.7) suggests that we can make V_Φ arbitrarily large by reducing K sufficiently. However, we obviously cannot make K so small that the SQUID has no influence on the tank circuit, and we need to establish a lower bound on K. Now to operate the SQUID, we must be able to choose a value of I_{rf} that intercepts the first step for all values of Φ : this requirement is satisfied if the point F in Fig. 10 lies to the right of E, that is if DF exceeds DE. We can calculate DF by noting that the power dissipation in the SQUID is zero at D and $\Delta E(\omega_{rf}/2\pi) \approx I_0\Phi_0\omega_{rf}/2\pi$ at F. Thus, $(I_{rf}^{(F)}-I_{rf}^{(D)})V_T^{(n+1/2)}/2 = I_0\Phi_0\omega_{rf}/2\pi$ (I_{rf} and V_T are peak, rather than rms values). Furthermore, we can easily see that $I_{rf}^{(E)} - I_{rf}^{(D)} = \Phi_0/2MQ$. Assuming $LI_0 \approx \Phi_0$ and using Eq.(4.5), we find that the requirement $I_{rf}^{(E)} > I_{rf}^{(D)}$ can be written in the form

$$K^2Q \gtrsim \pi/4. \tag{4.8}$$

If we set $K \approx Q^{-1/2}$, Eq.(4.7) becomes

$$V_\Phi \approx \omega_{rf}(QL_T/L)^{1/2}. \tag{4.9}$$

To operate the SQUID, one adjusts I_{rf} so that the SQUID remains biased on the first step (see Fig.10) for all values of Φ. The rf voltage across the tank circuit is amplified and demodulated to produce a signal that is periodic in Φ. A modulating flux, typically at 100kHz and with a peak-to-peak amplitude of $\Phi_0/2$, is also applied to the SQUID, just as in the case of the dc SQUID. The voltage produced by this modulation is lock-in detected, integrated, and fed-back as a current into the modulation coil to flux-lock the SQUID.

4.2 Theory of Noise in the rf SQUID

A detailed theory has been developed for noise in the rf SQUID;[46-54] in contrast to the case for the dc SQUID, noise contributions from the tank circuit and preamplifier are also important. We begin by discussing the intrinsic noise in the SQUID. In the previous section we assumed that transitions from the k=0 to the k=1 state occurred precisely at $\Phi = \Phi_C$. In fact, thermal activation causes the transition to occur stochastically, at lower values of flux. Kurkijärvi[46] calculated the distribution of values of Φ at which the transitions occur; experimental results[55] are in good agreement with his predictions. When the SQUID is driven with an rf flux, the fluctuations in the value of flux at which transitions occur have two consequences. First, noise is introduced on the peak voltage V_T, giving an equivalent intrinsic flux noise spectral density[47,51]

$$S_\Phi^{(i)} \approx \frac{(LI_0)^2}{\omega_{rf}}\left(\frac{2\pi k_B T}{I_0\Phi_0}\right)^{4/3}. \qquad (4.10)$$

Second, the noise causes the steps to tilt (Fig.11), as we can easily see by considering the case $\Phi = 0$. In the presence of thermal fluctuations the transition from to k = 0 to the k = 1 state (for example) has a certain probability of occurring at any given value of the total flux $\Phi + \Phi_{rf}$. Just to the right of A in Fig.10, this transition occurs at the peak of the rf flux once in many rf cycles. Thus, the probability of the transition occurring in any one cycle is small. On the other hand, at B a transition must occur at each positive and negative peak of the rf flux, with unity probability. To increase the transition probability, the peak value of the rf flux and hence V_T must increase as I_{rf} is increased from A to B. Jackel and Buhrman[48], introduced the slope parameter η defined in Fig.18, and showed that it was related to $S_\Phi^{(i)}$ by the relation

$$\eta^2 \approx S_\Phi^{(i)} \omega_{rf} / \pi \Phi_0^2 \qquad (4.11)$$

provided η was not too large. This relation is well-verified experimentally.

The noise temperature T_a of typical rf amplifiers operated at room temperature is substantially higher than that of amplifiers operated at a few hundred kilohertz, and is therefore not negligible for rf SQUIDs operated at liquid ^{4}He temperatures. Furthermore, part of the coaxial line connecting the tank circuit to the preamplifier is at room temperature. Since the capacitances of the line and the amplifier are a substantial fraction of the capacitance of the tank circuit, part of the resistance damping the tank circuit is well above the bath temperature. As a result there is an additional contribution to the noise which we combine with the preamplifier noise to produce an effective noise temperature T_a^{eff}. The noise energy contributed by these extrinsic sources can be shown to be[48,52] $2\pi\eta k_B T_a^{eff}/\omega_{rf}$. Combining this contribution with the intrinsic noise, one finds

$$\varepsilon \approx \frac{1}{\omega_{rf}} \left(\frac{\pi \eta^2 \Phi_0^2}{2L} + 2\pi\eta k_B T_a^{eff} \right). \qquad (4.12)$$

Equation (4.12) shows that ε scales as $1/\omega_{rf}$, but one should bear in mind that T_a tends to increase with ω_{rf}. Nonetheless, improvements in performance have been achieved by operating the SQUID at much higher frequencies[56,57] than the usual 20 or 30MHz. One can also reduce the T_a^{eff} by cooling the preamplifier,[56,58] thereby reducing T_a and reducing the temperature of the tank circuit to that of the bath. However, the best noise energies achieved for the rf

SQUID are substantially higher[59] than those routinely obtained with thin-film dc SQUIDs, and for this reason workers requiring the highest possible resolution almost invariably use the latter device.

4.3 Practical rf SQUIDs

Although less sensitive than the dc SQUID, the rf SQUID is entirely adequate for a wide range of applications. It is therefore more widely used than the dc SQUID, for the simple reason that reliable, easy-to-operate devices have been commercially available since the early 1970's, notably from BTi (formerly SHE). We shall therefore confine ourselves to a brief description of the device available from this company.

Figure 12 shows a cut-away drawing of the BTi rf SQUID[40], which has a toroidal configuration machined from Nb. One way to understand this geometry is to imagine rotating the SQUID in Fig.8 through 360° about a line running through the junction from top to bottom of the page. This procedure produces a toroidal cavity connected at its center by the junction. If one places a toroidal coil in this cavity, a current in the coil produces a flux that is tightly coupled to the SQUID. In Fig.12, there are actually two such cavities, one containing the tank circuit-modulation-feedback coil and the other the input coil. This separation eliminates cross-talk between the two coils. Leads to the two coils are brought out via screw-terminals. The junction is made from thin films of Nb. This device is self-shielding against external magnetic field fluctuations, and has proven to be reliable and convenient to use. In particular, the Nb input terminals enable one to connect different input circuits in a straightforward way. A typical device has a white noise energy of $5 \times 10^{-29} JHz^{-1}$, with a 1/f noise energy of perhaps $10^{-28} JHz^{-1}$ at 0.1Hz.

5. SQUID-BASED INSTRUMENTS

Both dc and rf SQUIDs are used as sensors in a far-ranging assortment of instruments. I here briefly discuss some of them: my selection is far from exhaustive, but does include the more commonly used instruments.

Each instrument involves a circuit attached to the input coil of the SQUID. We should recognize from the outset that, in general, the presence of the input circuit influences both the signal and noise properties of the SQUID while the SQUID, in turn, reflects a complex impedance into the input. Because the SQUID is a nonlinear device a full description of the interactions is complicated, and we shall not go into the details here. However, one aspect of this interaction, first pointed out by Zimmerman[60], is easy to understand. Suppose we connect a superconducting pick-up loop of inductance L_P to the input coil of inductance L_i to form a magnetometer, as shown in Fig.13(a). It is easy to show that the SQUID inductance L is reduced to the value

$$L' = L[1-\alpha^2 L_i/(L_i+L_P)], \qquad (5.1)$$

where α^2 is the coupling coefficient between L and L_i. We have neglected any stray inductance in the leads connecting L_i and L_P, and any stray capacitance. The reduction in L tends to increase the transfer coefficient of both the dc SQUID [Eq.(3.9)] and the rf SQUID [Eq.(4.9)]. In most cases, the reduction of L and the change in the noise properties will be detectable but will not have a major input on the results presented here.

5.1 Magnetometers and Gradiometers

One of the simplest instruments is the magnetometer [Fig.13(a)]. A pick-up loop is connected across the input coil to make a superconducting flux

transformer. The SQUID and input coil are generally enclosed in a superconducting shield. If one applies a magnetic flux, $\delta\Phi^{(p)}$, to the pick-up loop, flux quantization requires that

$$\delta\Phi^{(p)} + (L_i + L_p)J_S = 0, \tag{5.2}$$

where J_S is the supercurrent induced in the transformer. We have neglected the effects of the SQUID on the input circuit. The flux coupled into the SQUID, which we assume to be in a flux-locked loop, is $\delta\Phi = M_i|J_S| = M_i\delta\Phi^{(p)}/(L_i + L_P)$. We find the minimum detectable value of $\delta\Phi^{(p)}$ by equating $\delta\Phi$ with the equivalent flux noise of the SQUID. Defining $S_\Phi^{(p)}$ as the spectral density of the equivalent flux noise referred to the pick-up loop, we find

$$S_\Phi^{(p)} = \frac{(L_p+L_i)^2}{M_i^2} S_\Phi. \tag{5.3}$$

Introducing the equivalent noise energy referred to the pick-up loop, we obtain

$$\frac{S_\Phi^{(p)}}{2L_p} = \frac{(L_p+L_i)^2}{L_i\, L_p} \frac{S_\Phi}{2\alpha^2 L}. \tag{5.4}$$

We observe that Eq.(5.4) has the minimum value

$$\frac{S_\Phi^{(p)}}{2L_p} = \frac{4\varepsilon(f)}{\alpha^2} \tag{5.5}$$

when $L_i = L_p$. Thus, a fraction $\alpha^2/4$ of the energy in the pick-up loop is transferred to the SQUID. In this derivation we have neglected noise currents in

the input circuit arising from noise in the SQUID, the fact the the input circuit reduces the SQUID inductance, and any possible coupling between the feedback coil of the SQUID and the input circuit. Having obtained the flux resolution for $L_i = L_p$, we can immediately write down the corresponding magnetic field resolution $B_N^{(p)} = (S_\Phi^{(p)})^{1/2}/\pi r_p^2$, where r_p is the radius of the pick-up loop:

$$B_N^{(p)} = \frac{2\sqrt{2}L_p^{1/2}\varepsilon^{1/2}}{\pi r_p^2 \alpha}. \qquad (5.6)$$

Now[61] $L_p = \mu_0 r_p[\ln(8r_p/r_0)-2]$, where $\mu_0 = 4\pi \times 10^{-7}$ henries/meter and r_0 is the radius of the wire; for a reasonable range of values of r_p/r_0 we can set $L_P \approx 5\mu_0 r_p$. Thus we obtain $B_N^{(p)} \approx 2(\mu_0\varepsilon)^{1/2}/\alpha r_P^{3/2}$. This indicates that one can, in principle, improve the magnetic field resolution indefinitely by increasing r_p, keeping $L_i = L_p$. Of course, in practice, the size of the cryostat will impose an upper limit on r_p. If we take $\varepsilon = 10^{-28}$JHz^{-1} (a somewhat conservative value for an rf SQUID), $\alpha = 1$, and $r_P = 25$mm, we find $B_N^{(p)} \approx 5 \times 10^{-15}$ tesla Hz$^{-1/2}$ $= 5 \times 10^{-11}$ gauss Hz$^{-1/2}$. This is a much higher sensitivity than that achieved by any nonsuperconducting magnetometer.

Magnetometers have usually involved flux transformers made of Nb wire. For example, one can make the rf SQUID in Fig.12 into a magnetometer merely by connecting a loop of Nb wire to its input terminals. In the case of the thin-film dc SQUID, one can make an integrated magnetometer by fabricating a Nb loop across the spiral input coil. In this way, Wellstood et al.[18] achieved a magnetic field white noise of 5×10^{-15} tesla Hz$^{-1/2}$ with a pick-up loop a few millimeters across.

Magnetometers with typical sensitivities of 0.01 pTHz$^{-1/2}$ have been used in geophysics in a variety of applications,[62] for example, magnetotellurics, active

electromagnetic sounding, piezomagnetism, tectonomagnetism, and the location of hydrofractures. Although SQUID-based magnetometers are substantially more sensitive than any other type, the need to replenish the liquid helium in the field has restricted the extent of their applications. For this reason, the advent of high-temperature superconductors may have considerable impact on this field (see Sec.6).

An important variation of the flux transformer is the gradiometer. Figure 13(b) shows an axial gradiometer that measures $\partial B_z/\partial z$. The two pick-up loops are wound in opposition and balanced so that a uniform field B_z links zero net flux to the transformer. A gradient $\partial B_z/\partial z$, on the other hand, does induce a net flux and thus generates an output from the flux-locked SQUID. Figure 13(c) shows a second order gradiometer that measures $\partial^2 B_z/\partial z^2$; Fig.14(a) is a photograph of a practical version.

Thin-film gradiometers based on dc SQUIDs were made as long ago[28] as 1978, and a variety of devices[25,63-67] have been reported since then. To my knowledge, all of the gradiometers made to date have been planar, and therefore measure an off-diagonal gradient, for example, $\partial B_z/\partial x$ or $\partial^2 B_z/\partial x \partial y$. A representative device is shown in Fig.14(b)-(d).

The most important application of the gradiometer is in neuromagnetism[68], notably to detect weak magnetic signals emanating from the human brain. The gradiometer discriminates strongly against distant noise sources, which have a small gradient, in favor of locally generated signals. One can thus use a second-order gradiometer in an unshielded environment, although the present trend is towards using first-order gradiometers in a shielded room of aluminum and mu-metal that greatly attenuates the ambient magnetic noise. In this application, axial gradiometers of the type shown in Fig.13(a) actually sense magnetic field, rather than the gradient, because the distance from the signal

source to the pick-up loop is less than the baseline of the gradiometer. The magnetic field sensitivity referred to one pick-up loop is typically $10fTHz^{-1/2}$. Although great progress in this field has been made in recent years it is generally agreed that one needs an array of 50 to 100 gradiometers to make a clinically viable system. This requirement has greatly spurred the development of integrated, thin-film devices. For example, Knuutila[69] has reported that a 24-channel first-derivative array is under construction.

There are two basic kinds of measurements made on the human brain. In the first, one detects spontaneous activity: a classic example is the generation of magnetic pulses by subjects suffering from focal epilepsy[70]. The second kind involves evoked response: for example, Romani et al.[71] detected the magnetic signal from the auditory cortex generated by tones of different frequencies.

There are several other applications of gradiometers. One kind of magnetic monopole detector[72] consists of a gradiometer: the passage of a monopole would link a flux h/e in the pick-up loop and produce a step-function response from the SQUID. Gradiometers have recently been of interest in studies of corrosion and in the location of fractures in pipelines and other structures.

5.2 Susceptometers

In principle, one can easily use the first-derivative gradiometer of Fig.13(b) to measure magnetic susceptibility χ. One establishes a static field along the z-axis and lowers the sample into one of the pick-up loops. Provided χ is nonzero, the sample introduces an additional flux into the pick-up loop and generates an output from the flux-locked SQUID. A very sophisticated susceptometer is available commercially[73]. A room temperature access enables one to cycle samples rapidly, and one can measure χ as a function of temperature

between 1.8K and 400K in fields up to 5.5 tesla. The system is capable of resolving a change in magnetic moment as small as 10^{-8}emu.

Novel miniature susceptometers have been developed by Ketchen and co-workers[33,74,75]. One version is shown schematically in Fig.15. The SQUID loop incorporates two pick-up loops wound in the opposite sense and connected in series. The two square pick-up loops, 17.5μm on a side and with an inductance of about 30pH, are deposited over a hole in the ground plane that minimizes the inductance of the rest of the device. The SQUID is flux biased at the maximum of V_Φ by means of a control current I_C in one of the pick-up loops. One can apply a magnetic field to the two loops by means of the current I_F; by passing a fraction of this current into the center tap I_C, one can achieve a high degree of electronic balance between the two loops. The sample to be studied is placed over one of the loops, and the output from the SQUID when the field is applied is directly proportional to the magnetization. At 4.2K, the susceptometer is capable of detecting the magnetization due to as few as 3000 electron spins.
Awschalon and co-workers[33,75], have used a miniature susceptometer to perform magnetic spectroscopy of semiconductors with picosecond time-resolution.

5.3 Voltmeters

Probably the first practical application of a SQUID was to measure tiny, quasistatic voltages.[76] One simply connects the signal source --for example a low resistance through which a current can be passed-- in series with a known resistance and the input coil of the SQUID. The output from the flux-locked loop is connected across the known resistance to obtain a null-balancing measurement of the voltage. The resolution is generally limited by Nyquist noise in the input circuit, which at 4.2K varies from about 10^{-15}VHz$^{-1/2}$ for a resistance of $10^{-8}\Omega$ to about 10^{-10}VHz$^{-1/2}$ for a resistance of 100Ω.

Applications of these voltmeters range from the measurement of thermoelectric voltages and of quasiparticle charge imbalance in nonequilibrium superconductors to noise thermometry and the comparison of the Josephson voltage-frequency relation in different superconductors to high precision.

5.4 The dc SQUID as a Radiofrequency Amplifier

Over recent years, the dc SQUID has been developed into a low noise amplifier for frequencies up to 100MHz or more[77]. To understand the theory for the performance of this amplifier, we need to extend the theory of Sec.3 by taking into account the noise in the current J(t) in the SQUID loop. For a bare SQUID with $\beta = 1$, $\Gamma = 0.05$ and $\Phi = (2n+1)\Phi_0/4$ one finds the spectral density of the current to be[78]

$$S_J(f) \approx 11k_BT/R. \tag{5.7}$$

Furthermore, the current noise is partially correlated with the voltage noise across the SQUID, the cross-spectral density being[78]

$$S_{VJ}(f) \approx 12k_BT. \tag{5.8}$$

The correlation arises, roughly speaking, because the current noise generates a flux noise which in turn contributes to the total voltage noise across the junction provided $V_\Phi \neq 0$.

One can make a tuned amplifier, for example, by connecting an input circuit to the SQUID as shown in Fig.16. In general, the presence of this circuit modifies all of the SQUID parameters and the magnitude of the noise spectral densities[79]. Furthermore, the SQUID reflects an impedance $\omega^2M_i^2/Z$ into the input circuit[80], where Z is the dynamic input impedance of the SQUID. Fortunately, however, one can neglect the mutual influence of the SQUID and

input circuit provided the coupling coefficient α^2 is sufficiently small, as it is under certain circumstances. For a signal at frequency f generated by a source with resistance R_i one can optimize the noise temperature of the amplifier using standard procedures to obtain

$$T_N^{(opt)} = \frac{\pi f}{k_B V_\Phi} (S_V S_J - S_{VJ}^2)^{1/2}. \qquad (5.9)$$

This minimum value actually occurs off-resonance; if one wishes to operate the amplifer at the resonant frequency of the input circuit, the noise temperature is increased to

$$T_N^{(res)} = \frac{\pi f}{k_B V_\Phi} (S_V S_J)^{1/2}. \qquad (5.10)$$

The corresponding power gain is

$$G \approx V_\Phi/\omega. \qquad (5.11)$$

Equations (5.10) and (5.11) can be shown to imply $\alpha^2 Q \approx 1$, that is, the coupling is weak for a high-Q input circuit. We emphasize that the noise temperatures quoted in Eqs. (5.9) and (5.10) do not include the Nyquist noise generated in R_i, which may well exceed the noise generated by the amplifier. Thus, Eq. (5.9) or (5.10) does not necessarily represent the lowest system noise temperature, which may well occur under quite different conditions. Nonetheless, these expresions are very useful in that they specify the performance at a particular frequency in terms of the SQUID parameters only.

Hilbert and Clarke[77] made several radiofrequency amplifiers with both tuned and untuned inputs, flux biasing the SQUID near $\Phi = (2n+1)\Phi_0/4$. There was no flux-locked loop. The measured parameters were in good agreement with predictions. For example, for an amplifier with $R \approx 8\Omega$, $L \approx 0.4$nH, $L_i \approx 5.6$nH, $M_i \approx 1$nH and $V_\Phi \approx 3\times10^{10}$ sec^{-1} at 4.2K they found G = 18.6±0.5 dB and T_N = 1.7±0.5K at 93 MHz. The predicted values were 17dB and 1.1K, respectively.

To conclude this discussion, we comment briefly on the quantum limit of the dc SQUID amplifier. At T = 0, Nyquist noise in the shunt resistors in Eqs. (3.7) and (3.8) should be replaced with zero point fluctuations. Koch et al.[81] performed a simulation in this limit and concluded that, within the limits of error, the noise temperature of a tuned amplifier in the quantum limit should be given by

$$T_N \approx hf/k_B \ln 2. \qquad (5.12)$$

This is the result for any quantum limited amplifier. The corresponding value for ε was approximately $\hbar$, but it should be emphasized that quantum mechanics does not impose any precise lower limit on ε [82]. A number of SQUIDs have obtained noise energies of $3\hbar$ or less, but there is no evidence as yet that a SQUID has attained quantum limited performance as an amplifier.

Clarke, Hahn and co-workers[83-86] have used tuned SQUID amplifiers in a series of experiments to observe nuclear magnetic resonance (NMR) and nuclear quadruple resonance (NQR) at about 30 MHz. As an example of the high sensitivity offered by these techniques, they were able to detect "spin noise" in ^{35}Cl nuclei in $NaClO_3$. In zero magnetic field, this nucleus has two doubly degenerate nuclear levels with a splitting of 30.6856MHz and exhibits NQR. An rf signal at the NQR frequency equalized the populations of the two nuclear spin

levels, and was then turned off to leave a zero-spin state. A SQUID amplifier was able to detect the photons emitted spontaneously as the upper state decayed, even although the lifetime per nucleus against this process was ~10^6 centuries. The detected power was about $5x10^{-21}$W in a bandwidth of about 1.3kHz.

5.5 Gravity Wave Antennas

A quite different application of SQUIDs is to detect minute displacements, notably those of Weber bar gravity wave antennas.[87,88] Roughly a dozen groups worldwide are using these antennas to search for the pulse of gravitational radiation that is expected to be emitted when a star collapses. The radiation induces longitudinal oscillations in the large, freely suspended bar, but because the amplitude is very tiny, one requires the sensitivity of a dc SQUID to detect it. As an example, we briefly describe the antenna at Stanford University, which consists of an aluminum bar 3 meters long and weighing 4800kg suspended in a vacuum chamber at 4.2K. The fundamental longitudinal mode is at $\omega_a/2\pi \approx 842$Hz, and the Q is $5x10^6$. The transducer is shown schematically in Fig.17. A circular niobium diaphragm is clamped at its perimeter to one end of the bar, with a flat spiral coil made of niobium wire mounted on each side. The two coils are connected in parallel with each other and with the input coil of a SQUID; this entire circuit is superconducting. A persistent supercurrent circulates in the closed loop formed by the two spiral coils. The associated magnetic fields exert a restoring force on the diaphragm so that by adjusting the current, one can set the resonant frequency of the diaphragm equal to that of the bar. A longitudinal oscillation of the bar induces an oscillation in the position of the diaphragm relative to the two coils, thereby modulating their inductances. As a result of flux quantization, a fraction of the stored supercurrent is diverted into the input coil of the SQUID, which detects it in the usual way.

The present Stanford antenna has a root-mean-square strain sensitivity $<(\delta\ell)^2>^{1/2}/\ell$ of 10^{-18}, where ℓ is the length of the bar and $\delta\ell$ its longitudinal displacement. This very impressive sensitivity, which is limited by thermal noise in the bar, is nonetheless adequate only to detect events in our own galaxy. Because such events are rare, there is a very strong motivation to make major improvements in the sensitivity.

If the bar could be cooled sufficiently, the strain resolution would be limited only by the bar's zero-point motion and would have a value of about 3×10^{-21}. At first sight one might expect that the bar would have to be cooled to and absurdly low temperature to achieve this quantum limit, because a frequency of 842 Hz corresponds to a temperature $\hbar\omega_a/k_B$ of about 40nK. However, it turns out that one can make the effective noise temperature T_{eff} of the antenna much lower than the temperature T of the bar. If a gravitational signal in the form of a pulse of length τ_S interacts with an antenna that has a decay time Q/ω_a, then the effective noise temperature is given approximately by the product of the bar temperature and the pulse length divided by the decay time: $T_{eff} \approx \tau_S\omega_a T/Q$. Thus one can make the effective noise temperature much less than the temperature of the bar by increasing the bar's resonant quality factor sufficiently. To achieve the quantum limit, in which the bar energy $\hbar\omega_a$ is greater than the effective thermal energy $k_B T_{eff}$, one would have to lower the temperature T below $Q\hbar/k_B\tau_S$, which is about 40 mK for a quality factor Q of 5×10^6 and a pulse length τ_S of 1 msec. One can cool the antenna to this temperature with the aid of a large dilution refrigerator.

Needless to say, to detect the motion of a quantum-limited antenna one needs a quantum limited transducer, a requirement that has been the major driving force in the development of ultra-low-noise dc SQUIDs. As we have seen, however, existing dc SQUIDs at low temperatures are now within striking

distance of the quantum limit, and there is every reason to believe that one will be able to operate an antenna quite close to the quantum limit within a few years.

5.6 Gravity Gradiometers

The gravity gradiometer, which also makes use of a transducer to detect minute displacements, has been pioneered by Paik[89] and Mapoles[90]. The gradiometer consists of two niobium proof masses each constrained by springs to move along a common axis (Fig.18). A single-layer spiral coil of niobium wire is attached to the surface of one of the masses so that the surface of the wire is very close to the opposing surface of the other mass. Thus, the inductance of the coil depends on the separation of the two proof masses, which in turn depends on the gravity gradient. The coil is connected to a second superconducting coil which is coupled to a SQUID via a superconducting transformer. A persistent supercurrent, I, maintains a constant flux in the detector circuit. Thus, a change in the inductance of the pick-up coil produces a change in I and hence a flux in the SQUID that is related to the gravity gradient. More sophisticated versions of this design enable one to balance the restoring forces of the two springs electronically,[90] thereby eliminating the response to an acceleration (as opposed to an acceleration gradient). Sensitivities of a few Eötvös $Hz^{-1/2}$ have been achieved at frequencies above 2Hz.

Instruments of this kind could be used to map the earth's gravity gradient, and have potential in tests of the inverse square law and in inertial navigation.

6. THE IMPACT OF HIGH TEMPERATURE SUPERCONDUCTIVITY

The advent of the high transition temperature (T_C) superconductors[91] has stimulated great interest in the prospects for superconducting devices operating

at liquid (LN) temperatures (77K). Indeed, a number of groups have already successfully operated SQUIDs. In this section I shall give a brief overview of this work.

6.1 Predictions for White Noise

In designing a SQUID for operation at LN temperatures one must bear in mind the constraints imposed by thermal noise on the critical current and inductance, $I_0 \gtrsim 10\pi k_B T/\Phi_0$ and $L \lesssim \Phi_0^2/5k_B T$. For T =77K, we find $I_0 \gtrsim 16\mu A$ and $L \lesssim 0.8nH$. If we take as arbitrary but reasonable values L = 0.2nH and I_0 = 20μA, we obtain $2LI_0/\Phi_0 = 4$ for the dc SQUID and $LI_0/\Phi_0 = 2$ for the rf SQUID. These values are not too far removed from optimum, and to a first approximation we can use the equations for the noise energy given in Secs. 3 and 4.

For the case of the dc SQUID, the noise energy is predicted by either Eq.(3.11) or Eq.(3.12). However, since nobody has yet made a Josephson tunnel junction with high-T_C materials, it is somewhat unrealistic to use Eq.(3.12), which involves the junction capacitance, and instead we use Eq.(3.11). The value of R is an open question, and we rather arbitrarily adopt 5Ω, which is not too different from values achieved experimentally for high-T_C grain boundary junctions.[92] With L = 0.2nH, T = 77K and R = 5Ω, Eq.(3.11) predicts $\varepsilon \approx 4\times10^{-31}JHz^{-1}$. This value is only about one order of magnitude higher that that found at 4.2K for typical Nb-based, thin film dc SQUIDs, and actually somewhat better than that found in commercially available toroidal SQUIDs. These various values are summarized in Fig.19. If one could actually achieve the predicted resolution in a SQUID at 77K at frequencies down to 1Hz or less, it would be adequate for most of the applications discussed in Sec. 5.

For the rf SQUID, Eq.(4.10) predicts an intrinsic noise energy of about $6x10^{-29}JHz^{-1}$ for $I_0 = 20\mu A$, $LI_0 = 2\Phi_0$, $\omega_{rf}/2\pi = 20MHz$ and T = 77K. This value is comparable with the overall value obtained experimentally with 4.2K devices where the effective noise temperature T_a^{eff} of the preamplifier and tank circuit is much higher than the bath temperature when the preamplifier is at room temperature (see Sec.4.2). However, when one operates a SQUID at 77K, there is no reason for T_a^{eff} to increase and the system noise energy should be comparable with that at 4.2K.

With regard to 1/f noise, in general one might expect both critical current noise and flux noise to contribute. However, it seems impractical to make any a priori predictions of the magnitude of these contributions.

6.2 Practical Devices

Although a number of dc and rf SQUIDs have been made from YBCO, I shall describe just one of each type. It appears that the first dc SQUID was made by Koch et al.[92] In their first devices, they patterned the films by covering the regions of YBCO to remain superconducting with a gold film, and ion implanted the unprotected regions so that they became insulators at low temperatures. The configuration is shown in Fig.20; the estimated inductance is 80pH. The two microbridges exhibited Josephson-like behavior, which actually arose from junctions formed by grain boundaries between randomly oriented grains of YBCO. As the quality of the films has improved, conventional patterning techniques such as lift off and ion etching have become possible. The I-V characteristics of these devices are modulated by an applied flux, although the V-Φ curves are often hysteretic and nonperiodic, probably because of flux trapped in the YBCO films. The noise energy scaled approximately as 1/f over the

frequency range investigated, usually 1 to 10^3Hz. The lowest noise energies achieved to date at 1Hz are $4x10^{-27}JHz^{-1}$ at 41K and, in a different device, $2x10^{-26}J/Hz$ at 77K. These values are plotted in Fig.19.

The best characterized rf SQUID reported so far is that of Zimmerman et al.[93] They drilled a hole along the axis of a cylindrical pellet of YBCO, and cut a slot part way along a radius (Fig.21). The pellet was glued into an aluminum holder, also with a slot, and the assembly immersed in LN. A taper pin forced into the slot in the mount caused the YBCO to break in the region of the cut; when the pin was withdrawn slightly, the YBCO surfaces on the two sides of the crack were brought together, forming a "break junction". The rf SQUID so formed was coupled to a resonant circuit and operated in the usual way. The best flux resolution was $4.5x10^{-4}\Phi_0Hz^{-1/2}$ at 50Hz, corresponding to a noise energy of $1.6x10^{-27}JHz^{-1}$ for L = 0.25nH (see Fig.19).

6.3 Flux Noise in YBCO Films

It is evident that the l/f noise level in YBCO SQUIDs is very high compared with that in Nb or Pb devices at 4.2K. Ferrari et al.[94] have investigated the source of this noise by measuring the flux noise in YBCO films. Each film, deposited on a $SrTiO_3$ chip, was patterned into a loop and mounted parallel and very close to a Nb-based SQUID (with no input coil) so that any flux noise in the YBCO loop could be detected by the SQUID. The assembly was enclosed in a vacuum can immersed in liquid helium. The SQUID was maintained at 4.2K, while the temperature of the YBCO film could be increased by means of a resistive heater. Below T_C, the spectral density of the flux noise scaled as l/f over the frequency range 1 to 10^3Hz, and increased markedly with temperature. Three films were studied, with microstructure improving progressively with respect to the fraction of grains oriented with the c-axis perpendicular to the

substrate. The critical current density correspondingly increased, to a value of $2x10^6 Acm^{-2}$ at 4.2K in the best film. The spectral density of the noise measured at 1Hz is shown vs. temperature in Fig.22. We see that in each case the noise increases rapidly as the temperature approaches T_C, and that, at a given temperature, the noise decreases dramatically as the quality of the films is improved. The noise energy estimated at 28K and 77K with an assumed inductance of 400pH is shown in Fig.19.

The results demonstrate that YBCO films are intrinsically noisy. The noise presumably arises from the motion of flux quanta trapped in the films, possibly at grain boundaries. This mechanism is almost certainly the origin of the l/f noise observed in YBCO SQUIDs, and, in general terms, is similar to the origin of l/f noise in Nb SQUIDs. It is encouraging that the noise is reduced as the microstructure of the films is improved, and it should be emphasized that there is no reason to believe the lowest noise measured so far represents a lower bound. The implications are that SQUIDs and flux transformers coupled to them should be made of very high quality films.

6.4 Future Prospects for High-T_c SQUIDs

One potential application of a high-T_C SQUID is as a geophysical magnetometer (see Sec.5.1). At the moment, however, it is not entirely straightforward to predict the performance, since the devices are still evolving and it is evident from the noise measurements on YBCO films that thin-film flux transformers may introduce considerable levels of low frequency noise. To make some kind of estimate, we assume that we can optimally couple the 77K dc SQUID with the noise energy shown in Fig.19 to a noiseless flux transformer with a thin-film loop pick-up loop with a diameter of 50mm. The estimated loop inductance is about 150nH. Using Eq.(5.6), we find a magnetic field resolution

of roughly $0.1pTHz^{-1/2}$ at 1 Hz, improving to $0.01pTHz^{-1/2}$ at 100Hz. Although this performance is quite good, one should realize that commercially available coils operated at room temperature offer a resolution of about $0.03pTHz^{-1/2}$ over this frequency range. Furthermore, our assumption of a noise-free flux transformer is rather optimistic. Nonetheless, given the short time over which the high-T_C materials have been available one should be rather encouraged: a relatively modest reduction in the l/f noise that might be gained from improving the quality of YBCO films or even from using alternative materials might well yield a rather useful geophysical device.

One might note here that the real advantage in using liquid nitrogen as opposed to liquid helium for field applications is not really the reduction in cost, a savings which is negligible compared with the cost of mounting a field operation, but rather the very much slower boil-off rate of liquid nitrogen. The latent heat of vaporization of liquid N_2 is about 60 times that of liquid ^4He, so that one should be able to design cryostats of modest size with hold-times of up to a year. It is also noteworthy that liquid Ne, which boils at 27K, has a latent heat roughly 40 times that of liquid He, and its use would also greatly extend the running time over that of liquid He, for roughly the same cost per day. We see from Fig.22 that the l/f noise in YBCO films can be considerably lower at 27K than at 77K, so that the lower temperature operation could be a considerable advantage.

The likely impact of high-T_C SQUIDs on the more demanding applications such as neuromagnetism is much smaller, however, at least for the near future. Here, one needs very high sensitivity at frequencies down to 0.1Hz or less, but is not particularly concerned with the cost of liquid ^4He or the need to replenish it every day or two. Furthermore, low-noise, closed-cycle refrigerators are just becoming available that obviate the need to supply liquid cryogens in

environments where electrical power is available. Thus, it is difficult to imagine that high-T_C SQUIDs will have a significant impact in this area unless there is a major reduction in the l/f noise.

In concluding this section, we note that two key problems must be solved before high-T_C SQUIDs are likely to become technologically important. The first is the development of a reproducible and reliable Josephson junction. Although great progress has been made with grain boundary junctions, it is not clear that one can base a technology on this technique. Shiota et al.[95] have reported YBCO-insulator-YBCO junctions formed by fluorination of the base electrode, but the I-V characteristics revealed that one of the surfaces was normal. Hopefully, it will be possible to produce all-YBCO junctions exhibiting Josephson tunneling in the near future. An alternative might be a superconductor-normal metal metal-superconductor junction.[96] The second problem is concerned with the reduction of hysteresis and noise in thin films of high-T_C material. The motion of magnetic flux in the films is responsible for both effects, and one has to learn to produce films with lower densities of flux lines or higher pinning energies. Given the world-wide effort on the new superconductors, there is every reason to be optimistic about the long-term future of SQUIDs based on these materials.

7. CONCLUDING REMARKS

In this chapter I have tried to give an overview of the current status of dc and rf SQUIDs. I make no pretence that this account is comprehensive. There are many SQUID designs and applications that I have not mentioned, but I hope that I have given some flavor of the amazing versatility of these devices. For example, I find it remarkable that a dc SQUID is the basis of both the most

sensitive magnetometer available at 10^{-4}Hz and the quietest radio frequency amplifier at 10^{8}Hz.

The rf SQUID remains more widely used than the dc SQUID, simply because it is produced commercially and is thus available to people who are interested in using SQUIDs rather than in making them. One should also realize that although the kind of rf SQUID routinely used is much less sensitive than state-of-the-art thin-film dc SQUIDs, it is nonetheless entirely adequate for many applications. The fact that thin-film, integrated dc SQUIDs are not available commercially is presumably because the cost of establishing a facility to produce them is high while the perceived market is small. However, I suspect that this situation is about to change. After all, one needs only a single major application to make reasonably-priced SQUIDs available for any number of applications, and there now seem to be two such major products on the horizon. The first is in neuromagnetism: if this application is to become a clinical reality one will need systems with as many as100 channels, and the need for 100 channels will inevitably lead to the production of thin-film SQUIDs on a reasonable scale. The second is the advent of high-T_C thin-film SQUIDs. If these devices attain sufficient sensitivity and reliability for geophysical applications, not to mention laboratory-based applications such as voltmeters, they will be in sufficient demand to justify production on a commercial basis.

ACKNOWLEDGMENTS

I am indebted to D. Crum for supplying Fig. 14(a), P. F. Michelson Fig. 17, D. Paulsen Fig. 12, F. C. Wellstood Fig. 7, and J.E. Zimmerman Fig. 21. I wish to thank R. H. Koch and F. C. Wellstood for very helpful conversations. This work was supported by the Director, Office of Energy Research, Office of Basic Energy Sciences, Materials Sciences Division of the U.S. Department of Energy under contract number DE-AC03-76SF00098.

References

1. London. F.: Superfluids. Wiley, New York 1950
2. Josephson. B.D.: Possible new effects in superconductive tunneling. Phys. Lett. **1**. 251-253 (1962); Supercurrents through barriers. Adv. Phys. **14**. 419-451 (1965)
3. Jaklevic. R.C., Lambe. J., Silver. A.H., and Mercereau. J.E.: Quantum interference effects in Josephson tunneling. Phys. Rev Lett. **12**. 159-160 (1964)
4. Zimmerman. J.E., Thiene. P., Harding. J.T.: Design and operation of stable rf-biased superconducting point-contact quantum devices, and a note on the properties of perfectly clean metal contacts. J. Appl. Phys. **41**. 1572-1580 (1970)
5. Mercereau, J.E.: Superconducting magnetometers. Rev. Phys. Appl. **5**. 13-20 (1970); Nisenoff. M.: Superconducting magnetometers with sensitivities approaching 10^{-10} gauss. Rev. Phys. Appl. **5**. 21-24 (1970)
6. Stewart. W.C.: Current-voltage characteristics of Josephson junctions. Appl. Phys. Lett. **12**. 277-280 (1968)
7. McCumber. D.E.: Effect of ac impedance on dc voltage-current characteristics of Josephson junctions. J. Appl. Phys. **39**. 3113-3118 (1968).
8. Ambegaokar. V. and Halperin. B. I.: Voltage due to thermal noise in the dc Josephson effect. Phys. Rev. Lett. **22**. 1364-1366 (1969)
9. Clarke. J. and Koch. R. H.: The impact of high-temperature superconductivity on SQUIDs. Science **242**. 217-223 (1988)

10. Likharev. K. K. and Semenov. V. K.: Fluctuation spectrum in superconducting point junctions. Pis'ma Zh. Eksp. Teor. Fiz. **15.** 625-629 (1972). [JETP Lett. **15.** 442-445 (1972)]
11. Vystavkin. A. N., Gubankov. V.N., Kuzmin. L.S., Likharev. K.K., Migulin. V.V. and Semenov. V.K.: S-c-s junctions as nonlinear elements of microwave receiving devices. Phys. Rev. Appl. **9.** 79-109 (1974)
12. Koch. R.H., Van Harlingen. D.J. and Clarke. J.: Quantum noise theory for the resistively shunted Josephson junction. Phys. Rev Lett. **45.** 2132-2135 (1980)
13. Tesche. C.D. and Clarke. J.: dc SQUID: Noise and Optimization. J. Low. Temp. Phys. **27.** 301-331 (1977)
14. Bruines. J.J.P., de Waal. V.J. and Mooij. J.E.: Comment on "dc SQUID noise and optimization" by Tesche and Clarke. J. Low. Temp. Phys. **46.** 383-386 (1982)
15. De Waal. V.J., Schrijner. P. and Llurba. R. Simulation and optimization of a dc SQUID with finite capacitance. J. Low. Temp. Phys. **54.** 215-232 (1984)
16. Ketchen. M.B. and Jaycox. J.M.: Ultra-low noise tunnel junction dc SQUID with a tightly coupled planar input coil. Appl. Phys. Lett. **40.** 736-738 (1982)
17. Jaycox J.M. and Ketchen M.B.: Planar coupling scheme for ultra low noise dc SQUIDs. IEEE Trans. Magn., **MAG- 17.** 400-403 (1981)
18. Wellstood. F.C., Heiden. C. and Clarke. J.: Integrated dc SQUID magnetometer with high slew rate. Rev. Sci. Inst. **55.** 952-957 (1984)
19. Gurvitch. M., Washington. M.A. and Huggins. H.A.: High quality refactory Josephson tunnel junction utilizing thin aluminum layers. Appl. Phys. Lett. **42.** 472-474 (1983)

20. De Waal. V.J., Klapwijk. T.M. and Van den Hamer. P.: High performance dc SQUIDs with submicrometer niobium Josephson junctions. J. Low. Temp. Phys. **53**. 287-312 (1983)

21. Tesche. C.D., Brown. K.H., Callegari. A.C., Chen. M.M., Greiner. J.H., Jones. H.C., Ketchen. M.B., Kim. K.K., Kleinsasser. A.W., Notarys. H.A., Proto. G., Wang. R.H. and Yogi. T.: Practical dc SQUIDs with extremely low l/f noise. IEEE Trans. Magn. **MAG-21.** 1032-1035 (1985)

22. Pegrum. C.M., Hutson. D., Donaldson. G.B. and Tugwell. A.: DC SQUIDs with planar input coils. ibid. 1036-1039 (1985)

23. Noguchi. T., Ohkawa. N. and Hamanaka. K.: Tunnel junction dc SQUID with a planar input coil. SQUID 85 Superconducting Quantum Interference Devices and their Applications. Ed. Hahlbohm. H. D. and Lubbig. H. (Walter de Gruyter, Berlin, 1985) 761-766

24. Muhlfelder. B., Beall. J.A., Cromar. M.W. and Ono. R.H.: Very low noise tightly coupled dc SQUID amplifiers. Appl. Phys. Lett. **49**. 1118-1120 (1986)

25. Knuutila. J., Kajola. N., Seppä. H., Mutikainen. R. and Salmi. J.: Design, optimization and construction of a dc SQUID with complete flux transformer circuits. J. Low. Temp. Phys. **71**. 369-392 (1988)

26. Carelli. P. and Foglietti. V.: Behavior of a multiloop dc superconducting quantum interference device. J. Appl. Phys. **53**. 7592-7598 (1982)

27. Clarke. J., Goubau. W.M. and Ketchen. M.B.: J. Low. Temp. Phys. **25**. 99-144 (1976)

28. Ketchen. M.B., Goubau. W.M., Clarke. J. and Donaldson. G.B.: Superconducting thin-film gradiometer. J. Appl. Phys. **44**. 4111-4116 (1978)

29. Wellstood. F.C., and Clarke. J.: unpublished.

30. Wellstood. F.C., Urbina. C. and Clarke. J.: Low-frequency noise in dc superconducting quantum interference devices below 1K. Appl. Phys. Lett. **50**. 772-774 (1987)

31. Roukes. M. L., Freeman. M. R., Germain. R. S., Richardson. R. C. and Ketchen. M. B.: Hot electrons and energy transport in metals at millikelvin temperatures. Phys. Rev. Lett. **55.** 422-425 (1985)

32. Wellstood. F.C., Urbina. C. and Clarke. J.: Hot electron effect in the dc SQUID. Proceedings of the Applied Superconductivity Conference August 21-25 1988 (to be published).

33. Ketchen. M.B., Awschalom. D.D., Gallagher. W.J., Kleinsasser. A.W., Sandstrom. R.L., Rozen. J.R. and Bumble. B.: Design, fabrication and performance of integrated miniature SQUID susceptometers. Proceedings of the Superconductivity Conference August 21-25 1988 (to be published).

34. Koch. R.H., Clarke. J., Goubau. W.M., Martinis. J.M., Pegrum. C.M. and Van Harlingen. D.J.: Flicker (l/f) noise in tunnel junction dc SQUIDs. J. Low. Temp. Phys. **51**. 207-224 (1983)

35. Rogers. C.T. and Buhrman. R.A.: Composition of l/f noise in metal-insulator-metal tunnel junctions. Phys. Rev. Lett. **53**. 1272-1275 (1984)

36. Dutta. P. and Horn. P.M.: Low-frequency fluctuations in solids: l/f noise. Rev. Mod. Phys. **53**. 497-516 (1981)

37. Van der Ziel. A.: On the noise spectra of semi-conductor noise and of flicker effect. Physica. **16**. 359-372 (1950)

38. Tesche. C.D., Brown. R. H., Callegari. A. C., Chen. M. M., Greiner. J. H., Jones. H. C., Ketchen. M. B., Kim. K. K., Kleinsasser. A. W., Notarys. H. A., Proto. G., Wang. R. H. and Yogi. T.: Well-coupled dc SQUID with

extremely low l/f noise. Proc. 17th International Conference on low temperature physics LT-17. (North Holland, Amsterdam 1984) 263-264

39. Foglietti. V, Gallagher. W. J., Ketchen. M. B., Kleinsasser. A. W., Koch. R. H., Raider. S. I. and Sandstrom. R. L.: Low-frequency noise in low l/f noise dc SQUIDs. Appl. Phys. Lett. **49**. 1393-1395 (1986).

40. Biomagnetic Technologies Inc. 4174 Sorrento Valley Blvd., San Diego, CA 92121.

41. Fujimaki. N., Tamura. H., Imamura. T. and Hasuo. S.: A single-chip SQUID magnetometer. Digest of Tech. papers of 1988 International Solid-state conference. (ISSCC) San Francisco. pp. 40-41. A longer version with the same title is to be published.

42. Drung. D.: Digital Feedback loops for dc SQUIDs. Cryogenics **26.** 623-627 (1986). Drung. D., Crocoll. E., Herwig. R., Neuhaus. M. and Jutzi. W.: Measured performance parameters of gradiometers with digital output. Proceedings of the Applied Superconductivity Conference, August 21-25 1988 (to be published).

43. Mück. M. and Heiden. C.: Simple dc SQUID system based on a frequency modulated relaxation oscillator. Proceedings of the Applied Superconductivity Conference, August 21-25 1988 (to be published).

44. Clarke. J.: Superconducting QUantum Interference Devices for Low Frequency Measurements. Superconductor Applications : SQUIDs and Machines, Ed. Schwartz. B. B.and Foner. S. (Plenum New York 1977). pp 67-124.

45. Giffard. R. P., Webb. R.A. and Wheatley. J.C.: Principles and methods of low-frequency electric and magnetic measurements using rf-biased point-contact superconducting device. J. Low. Temp. Phys. **6**. 533-610 (1972)

46. Kurkijärvi. J.: Intrinsic fluctuations in a superconducting ring closed with a Josephson junction. Phys. Rev. B **6**. 832-835 (1972)

47. Kurkijärvi. J. and Webb. W.W.: Thermal noise in a superconducting flux detector. Proc. Applied Superconductivity Conf. (Annapolis, MD.) 581-587 (1972)

48. Jackel. L.D. and Buhrman. R.A.: Noise in the rf SQUID. J. Low. Temp. Phys. **19**. 201-246 (1975)

49. Ehnholm. G.J.: Complete linear equivalent circuit for the SQUID. SQUID Superconducting Quantum Interference Devices and their Applications. Ed. Hahlbohm. H.D. and Lubbig. H. (Walter de Gruyter, Berlin, 1977) 485-499; Theory of the signal transfer and noise properties of the rf SQUID. J. Low. Temp. Phys. **29**. 1-27(1977)

50. Hollenhorst. H.N. and Giffard. R.P.: Input noise in the hysteretic rf SQUID: theory and experiment. J. Appl. Phys. **51**. 1719-1725 (1980)

51. Kurkijärvi. J.: Noise in the superconducting flux detector. J. Appl. Phys. **44**. 3729-3733 (1973)

52. Giffard. R.P., Gallop. J.C. and Petley. B.N.: Applications of the Josephson effects. Prog. Quant. Electron **4**. 301-402 (1976)

53. Ehnholm. G.J., Islander. S.T., Ostman. P. and Rantala. B.: Measurements of SQUID equivalent circuit parameters. J. de Physique **39**. colloque C6. 1206-1207 (1978)

54. Giffard. R.P. and Hollenhorst. J.N.: Measurement of forward and reverse signal transfer coefficients for an rf-biased SQUID. Appl. Phys. Lett. **32**. 767-769 (1978)

55. Jackel. L. D., Webb. W. W., Lukens. J. E. and Pei. S. S.: Measurement of the probability distribution of thermally excited fluxoid quantum

transitions in a superconducting ring closed by a Josephson junction. Phys. Rev. **B9**. 115-118 (1974)

56. Long. A., Clark. T. D., Prance. R. J. and Richards. M. G.: High performance UHF SQUID magnetometer. Rev. Sci. Instrum. **50**. 1376-1381 (1979)

57. Hollenhorst. J. N. and Giffard. R. P.: High sensitivity microwave SQUID. IEEE Trans. Magn. **MAG-15**. 474-477 (1979)

58. Ahola. H., Ehnholm. G. H., Rantala. B. and Ostman. P.: Cryogenic GaAs-FET amplifiers for SQUIDs. J. de Physique **39**. colloque C6. 1184-1185 (1978); J. Low Temp. Phys. **35**. 313–328 (1979)

59. For a review, see Clarke. J.: Advances in SQUID Magnetometers. IEEE Trans. Election Devices. **ED-27**.1896-1908 (1980)

60. Zimmerman. J. E.: Sensitivity enhancement of Superconducting Quantum Interference Devices through the use of fractional-turn loops. J. Appl. Phys. **42**. 4483-4487 (1971)

61. Shoenberg. D.: Superconductivity (Cambridge University Press 1962) 30.

62. For a review, see Clarke. J.: Geophysical Applications of SQUIDs. IEEE Trans. Magn. **MAG-19**. 288-294 (1983)

63. De Waal. V. J. and Klapwijk. T. M.: Compact Integrated dc SQUID gradiometer. Appl. Phys. Lett. **41**. 669-671 (1982)

64. Van Nieuwenhuyzen G. J. and de Waal. V. J.: Second order gradiometer and dc SQUID integrated on a planar substrate. Appl. Phy. Lett. **46**. 439-441 (1985)

65. Carelli. P. and Foglietti. V.: A second derivative gradiometer integrated with a dc superconducting interferometer. J. Appl. Phys. **54**. 6065-6067 (1983)

66. Koyangi. M., Kasai. N., Chinore. K., Nakanishi. M. and Kosaka. S.: An integrated dc SQUID gradiometer for biomagnetic application. Proceedings of the Applied Superconductivity Conference August 21-25, 1988 (to be published)

67. Knuutila. J., Kajola. M., Mutikainen. R., Salmi. J.: Integrated planar dc SQUID magnetometers for multichannel neuromagnetic measurements. Proc. ISEC '87 p. 261

68. For reviews, see Romani. G. L., Williamson. S. J. and Kaufman. L.: Biomagnetic instrumentation. Rev. Sci. Instrum. **53**. 1815-1845 (1982); Buchanan. D. S., Paulson. D. and Williamson. S. J.: Instrumentation for clinical applications of neuromagnetism. Adv. Cryo. Eng. (to be published)

69. Knuutila. J.: European Physical Society Workshop "SQUID: State of Art, Perspectives and Applications". Rome, Italy June 22-24, 1988 (unpublished)

70. Barth. D. S., Sutherling. W., Engel. J. Jr. and Beatty J.: Neuromagnetic evidence of spatially distributed sources underlying epileptiform spikes in the human brain. Science **223.** 293-296 (1984)

71. Romani. G. L., Williamson. S. J. and Kaufman. L.: Tonotopic organization of the human auditory cortex. Science **216.** 1339-1340 (1982)

72. Cabrera. B.: First results from a superconductive detector for moving magnetic monopoles. Phys. Rev. Lett. **48**. 1378-1381 (1982)

73. Quantum Design, 11568 Sorrento Valley Road, San Diego, CA 92121.

74. Ketchen. M. B., Kopley. T. and Ling. H.: Minature SQUID susceptometer. Appl Phys. Lett. **44.** 1008-1010 (1984)

75. Awschalom. D. D. and Warnock. J.: Picosecond magnetic spectroscopy with integrated dc SQUIDs. Proceedings of the Applied Superconductivity Conference August 21-25, 1988 (to be published)

76. Clarke. J.: A superconducting galvanometer employing Josephson tunneling. Phil. Mag. **13.** 115-127 (1966)

77. Hilbert. C. and Clarke. J.: DC SQUIDs as radiofrequency amplifiers. J. Low Temp. Phys. **61.** 263-280 (1985)

78. Tesche. C. D. and Clarke. J.: DC SQUID: current noise. J. Low Temp. Phys. **37.** 397-403 (1979)

79. Hilbert. C. and Clarke. J.: Measurements of the dynamic input impedance of a dc SQUID. J. Low Temp. Phys. **61.** 237-262 (1985)

80. Martinis. J. M. and Clarke. J.: Signal and noise theory for the dc SQUID. J. Low Temp. Phys. **61.** 227-236 (1985), and references therein.

81. Koch. R.H., Van Harlingen. D. J. and Clarke. J.: Quantum noise theory for the dc SQUID. Appl. Phys. Lett. **38.** 380-382 (1981)

82. Danilov. V. V., Likharev. K. K. and Zorin. A. B.: Quantum noise in SQUIDs. IEEE Trans. Magn. **MAG-19.** 572-575 (1983)

83. Hilbert. C., Clarke. J., Sleator. T. and Hahn. E. L.: Nuclear quadruple resonance detected at 30MHz with a dc superconducting quantum interference device. Appl. Phys. Lett. **47.** 637-639 (1985). (See references therein for earlier work on NMR with SQUIDS).

84. Fan. N. Q., Heaney. M.B., Clarke. J., Newitt. D., Wald. L. L., Hahn. E. L., Bielecke. A. and Pines. A.: Nuclear magnetic resonance with dc SQUID preamplifiers. Proceedings of the Applied Superconductivity Conference August 21–25 (1988)

85. Sleator. T., Hahn. E. L., Heaney, M.B., Hilbert. C. and Clarke. J.: Nuclear electric quadrupole induction of atomic polarization. Phys. Rev. Lett. **57.** 2756-2759 (1986)

86. Sleator. T., Hahn. E. L., Hilbert, C. and Clarke. J.: Nuclear-spin noise and spontaneous emission. Phys. Rev. B. **36.** 1969-1980 (1987)

87. For an elementary review on gravity waves, see Shapiro. S. L., Stark. R.F. and Teukolsky. S. J.: The search for gravitational waves. Am. Sci. **73.** 248-257 (1985)

88. For a review on gravity-wave antennae, see Michelson. P. F., Price. J. C. and Taber. R. C.: Resonant-mass detectors of gravitational radiation. Science **237**.150-157 (1987)

89. Paik. H. J.: Superconducting tensor gravity gradiometer with SQUID readout. SQUID Applications to Geophysics. Ed. Weinstock H. and Overton. W. C., Jr. (Soc. of Exploration Geophysicists, Tulsa, Oklahoma, 1981) 3-12

90. Mapoles. E.: A superconducting gravity gradiometer. ibid. 153-157

91. Bednorz. J. G. and Muller. K. A.: Possible high T_c superconductivity in the Ba-La-Cu-O system. Z. Phys. **B64.** 189-193 (1986)

92. Koch. R. H., Umbach. C. P., Clark. G. J., Chaudhari. P. and Laibowitz. R. B.: Quantum interference devices made from superconducting oxide thin films. Appl. Phys. Lett. **51.** 200-202 (1987)

93. Zimmerman. J. E., Beall. J. A., Cromar. M. W. and Ono. R. H.: Operation of a Y-Ba-Cu-O rf SQUID at 81K. Appl. Phys. Lett. **51.** 617-618 (1987)

94. Ferrari. M. J., Johnson. M., Wellstood. F. C., Clarke. J., Rosenthal. P. A., Hammond. R. H. and Beasley. M. R.: Magnetic flux noise in thin film rings of $YBa_2Cu_3O_{7-\delta}$. Appl. Phys. Lett. **53.** 695-697 (1988)

95. Shiota. T., Takechi. K., Takai. Y and Hayakawa. H.: An observation of quasiparticle tunneling characteristics in all Y-Ba-Cu-0 thin film tunnel junctions (unpublished)

96. Mankiewich. P. M., Schwartz. D. B., Howard. R. E., Jackel. L. D., Straughn. B. L., Burkhardt. E. G. and Dayem. A. H.: Fabrication and characterization of an $YBa_2Cu_30_7/Au/YBa_2Cu_30_7$ S-N-S microbridge. Fifth International Workshop on Future Electron Devices - High Temperature Superconducting Devices. June 2-4, 1988, Miyaki-Zao, Japan. 157-160

Figure captions

Fig. 1(a) The resistively shunted Josephson junction; (b) and (c) show the tilted washboard model for $I<I_0$ and $I>I_0$.

Fig. 2(a) The dc SQUID; (b) I-V characteristics; (c) V vs. Φ/Φ_0 at constant bias current I_B.

Fig.3(a) Configuration of planar dc SQUID with overlaid spiral input coil; (b) expanded view of junctions and shunts.

Fig.4(a) Photograph of planar dc SQUID made at UC Berkeley, with 50-turn input coil; the square washer is about 1 mm across. (b) Electron micrograph of junctions prior to deposition of counterelectrode; each junction is about 3 μm across.

Fig. 5 Flux modulation scheme showing voltage across the SQUID for (a) $\Phi = n\Phi_0$ and (b) $\Phi = (n+1/4)\Phi_0$. The output V_L from the lock-in detector vs. Φ is shown in (c).

Fig. 6 Modulation and feedback circuit for the dc SQUID.

Fig.7 Spectral density of equivalent flux noise for dc SQUID with a Pb body : L = 0.2nH, R = 8Ω, and T = 4.2K. (Courtesy F.C. Wellstood).

Fig.8 The rf SQUID inductively coupled to a resonant tank circuit.

Fig.9 The rf SQUID: (a) total flux Φ_T vs. Φ for $LI_0 = 1.25\ \Phi_0$; (b) values of Φ_T as Φ is quasistatically increased and then decreased.

Fig.10 V_T vs. I_{rf} in the absence of thermal noise for $\Phi = n\Phi_0$, $(n+1/2)\Phi_0$.

Fig.11 V_T vs. I_{rf} showing the effects of thermal noise.

Fig.12 Cut-away drawing of toroidal SQUID (courtesy BTi, inc.).

Fig.13 Superconducting flux transformers:(a) magnetometer, (b) first-derivative gradiometer, (c) second-derivative gradiometer.

Fig.14 (a) Photograph of wire-wound second-derivative gradiometer for biomedical applications (courtesy BTi, inc.); thin-film first-derivative gradiometer: (b) pick-up loops, (c) two-hole SQUID with spiral input coils, and (d) expanded view of the dotted circle in (c) showing junctions and resistive shunts (from ref. 66).

Fig.15 Thin-film miniature susceptometer (from ref. 74).

Fig.16 Tuned radiofrequency amplifier based on dc SQUID (from ref.77).

Fig.17 Transducer for gravity wave antenna (courtesy P.F. Michelson).

Fig.18 Gravity gradiometer showing two proof masses (M) on either side of a planar spiral coil (from ref. 90).

Fig.19 Noise energy $\varepsilon(f)$ vs. frequency for several SQUIDs and for a YBCO film.

Fig.20 Planar thin-film dc SQUID fabricated from YBCO (re-drawn from ref. 92).

Fig. 21 Break-junction rf SQUID (from ref. 93).

Fig.22 Spectral density of flux noise at 1Hz vs. temperature for three YBCO films: polycrystalline (squares), mixed a- and c-axis (triangles) and >90% c-axis (circles). Solid symbols indicate the

noise is 1/f at 1Hz, open that it is white or nearly white (from ref. 94).

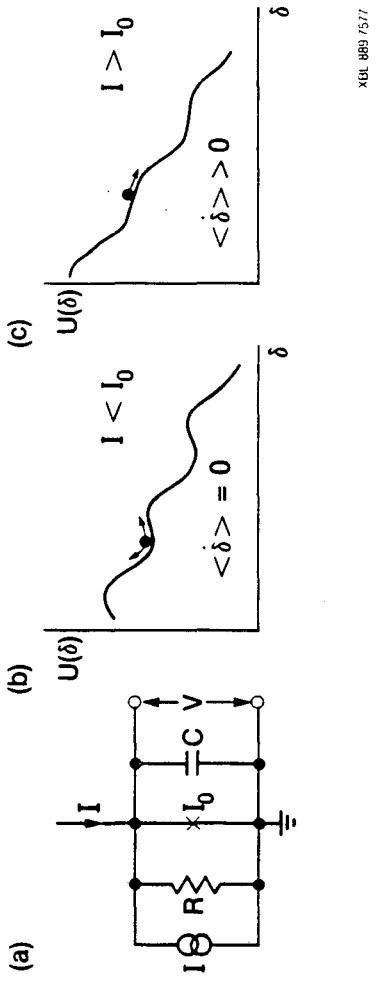
(a)
I
I_0
C
V
R
I_Θ
(b)
U(δ)
$I < I_0$
$\langle \dot{\delta} \rangle = 0$
δ
(c)
U(δ)
$I > I_0$
$\langle \dot{\delta} \rangle > 0$
δ
XBL 889 7577

Fig. 1

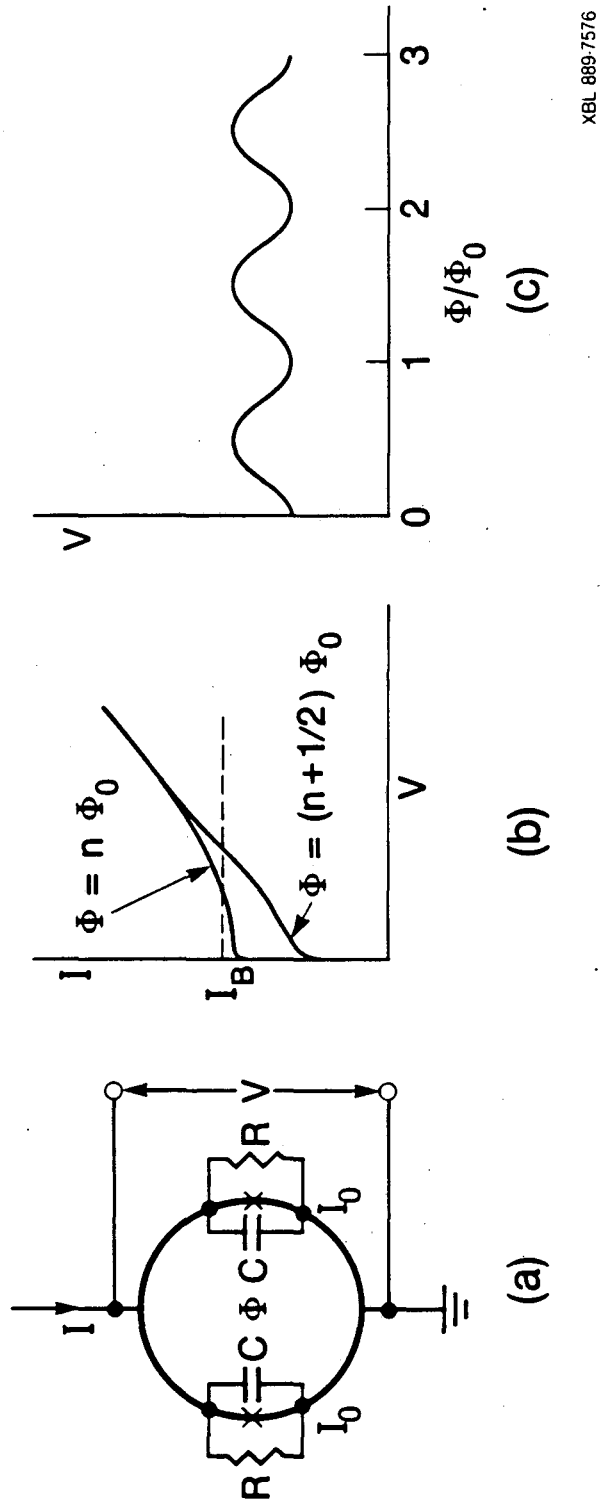

Fig. 2

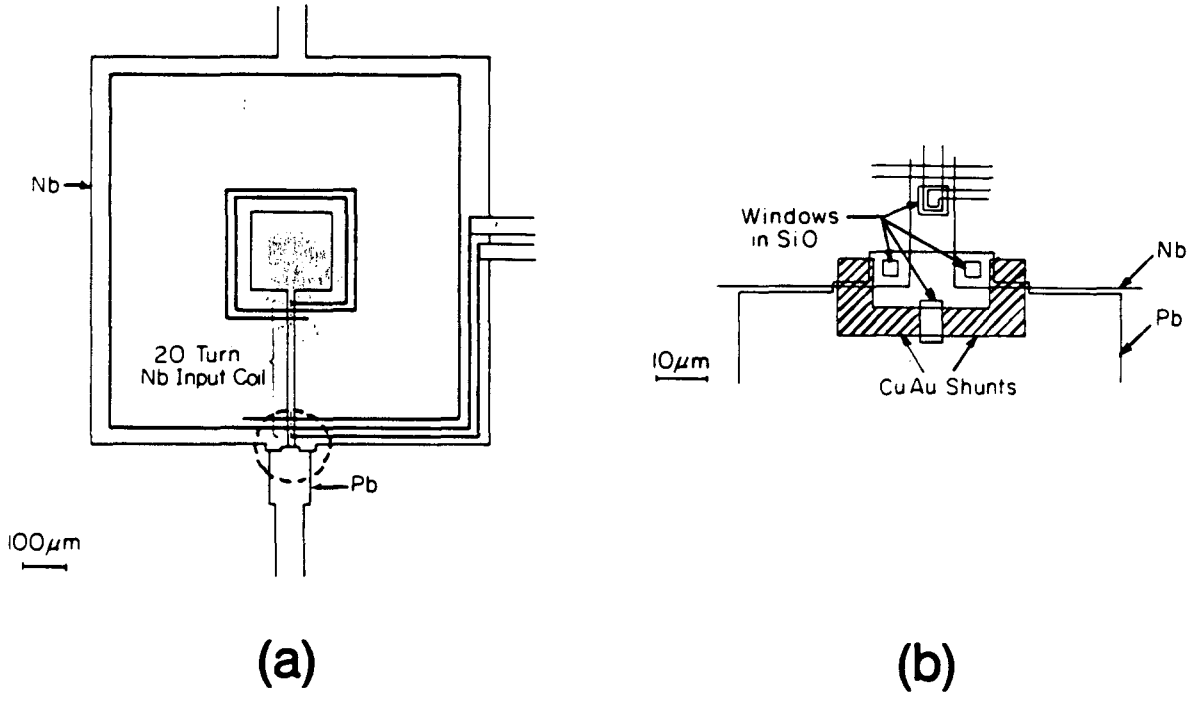

XBL 889-7581

Fig. 3

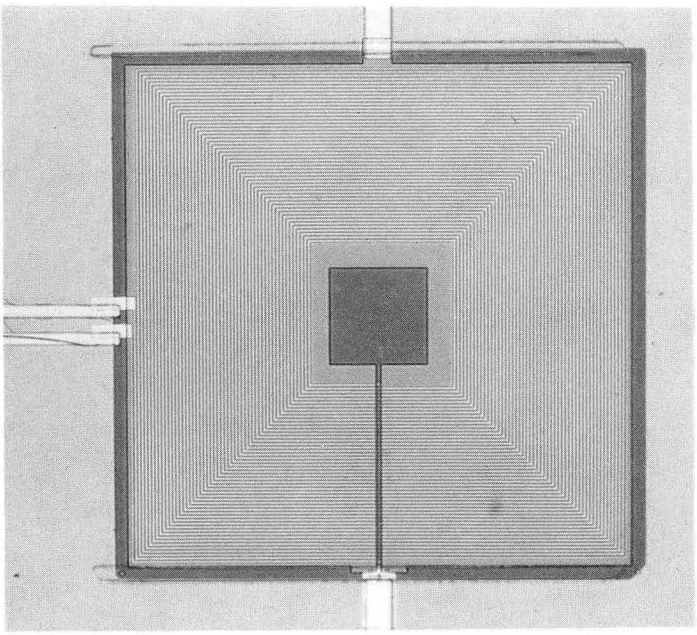

CBB 837-5927

(a)

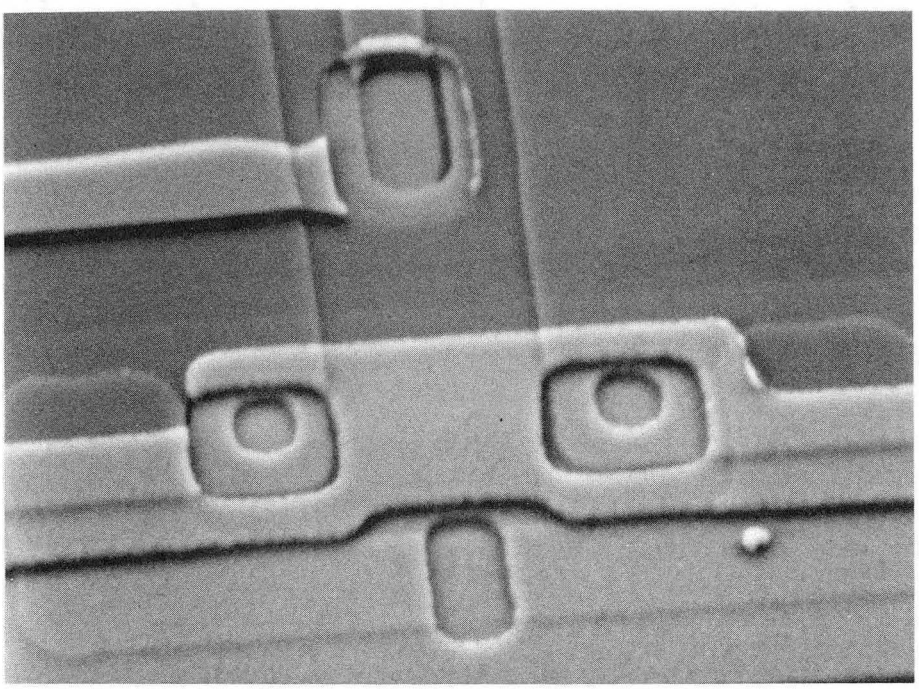

XBB 850-9959

(b)

Fig. 4

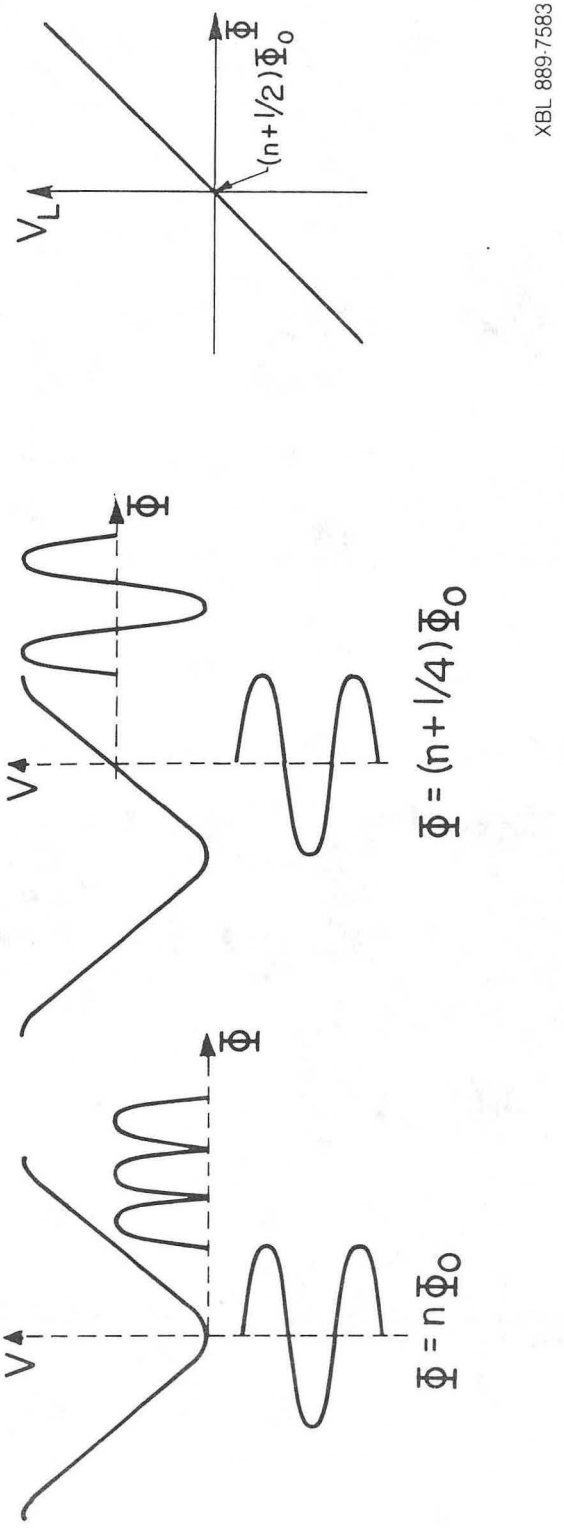

XBL 889-7583

Fig. 5

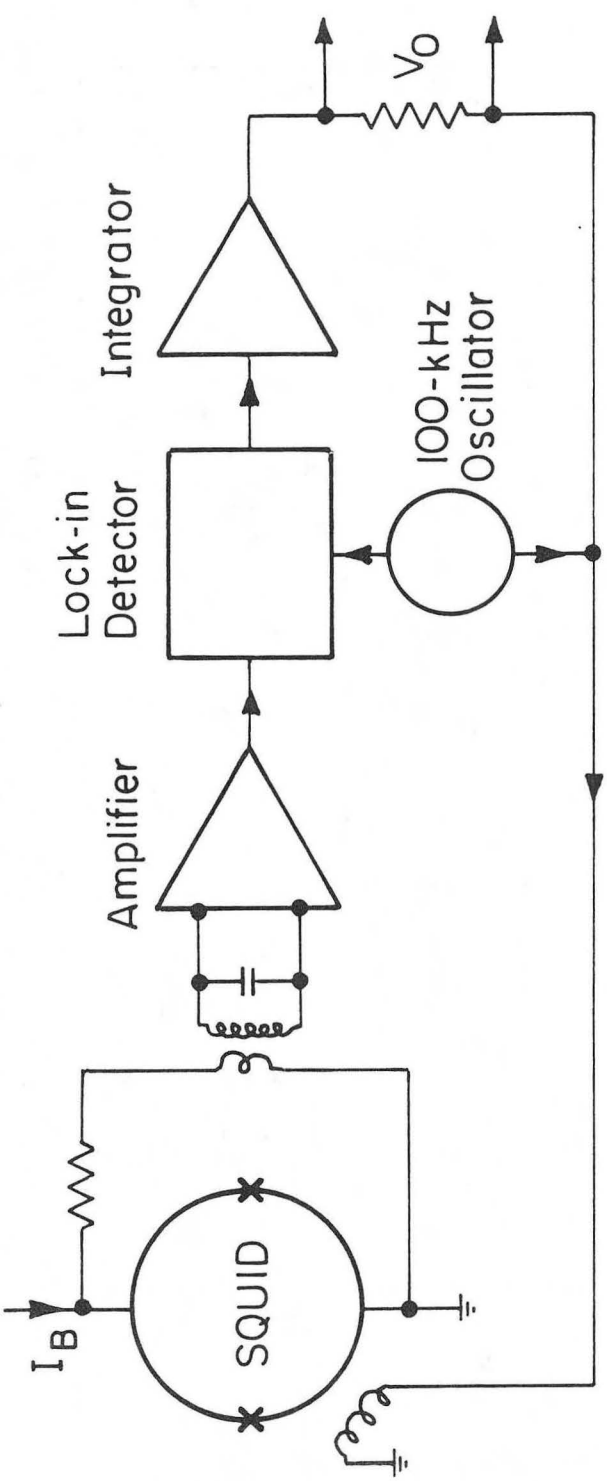

XBL 818-6302

Fig. 6

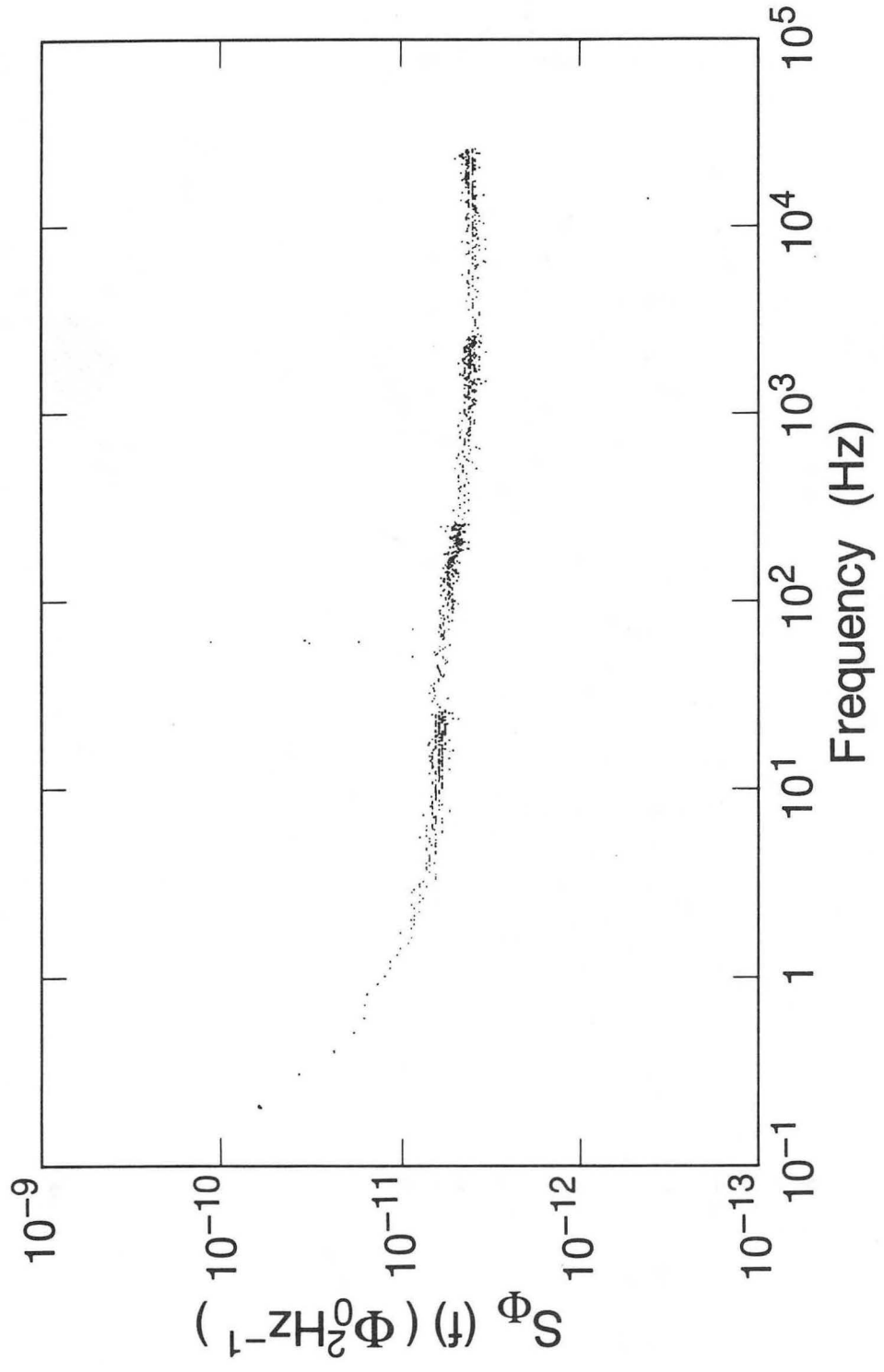

XBL 889 7595

Fig. 7

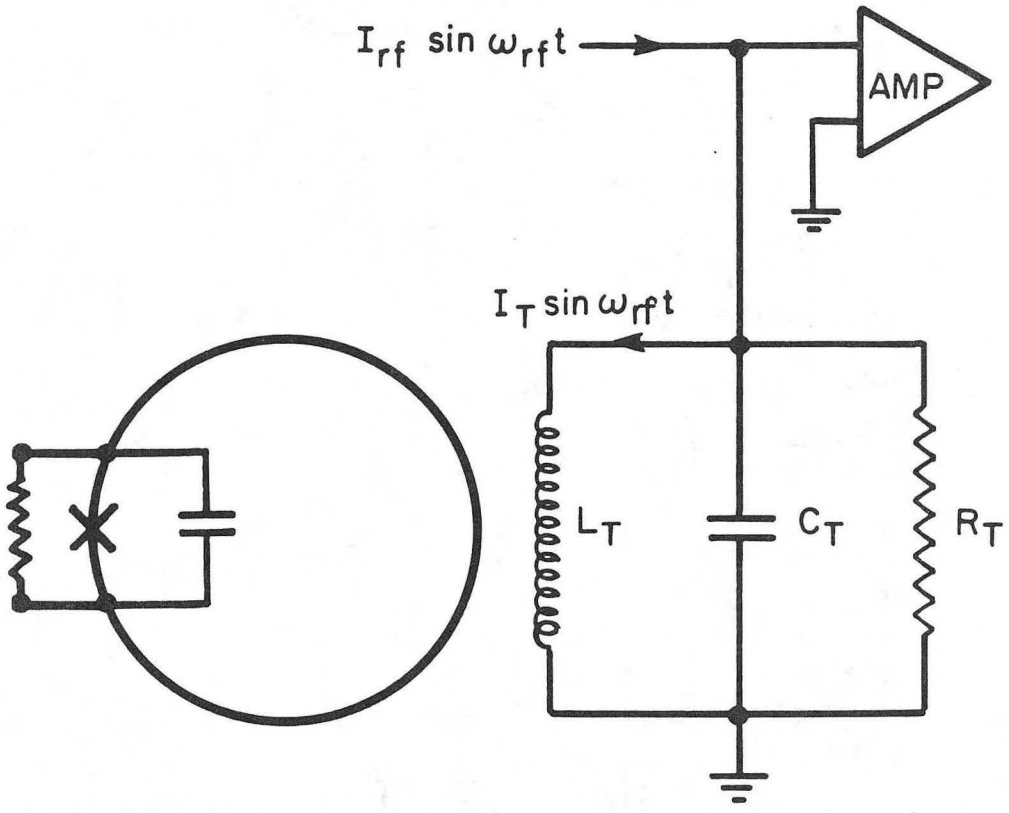

XBL 766-7133A

Fig. 8

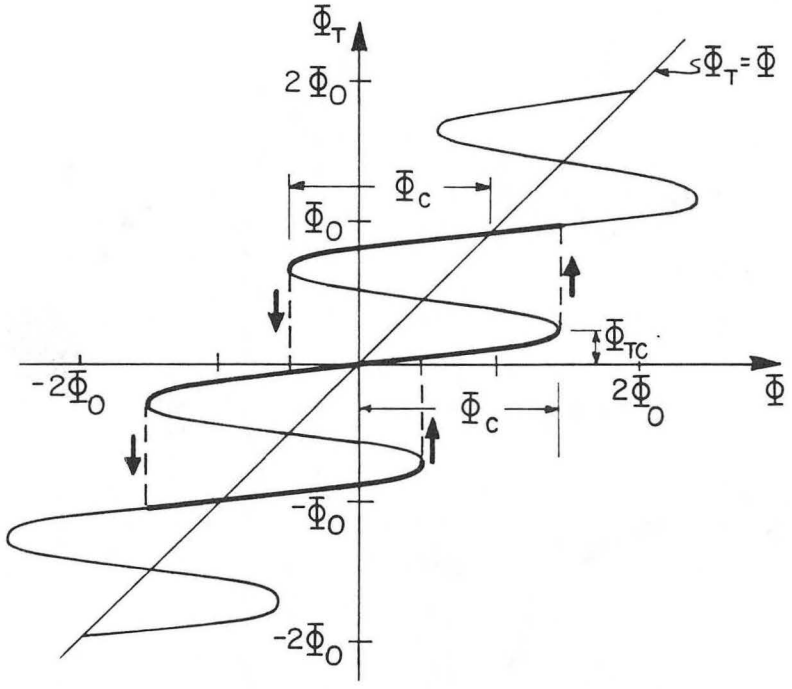

(a)

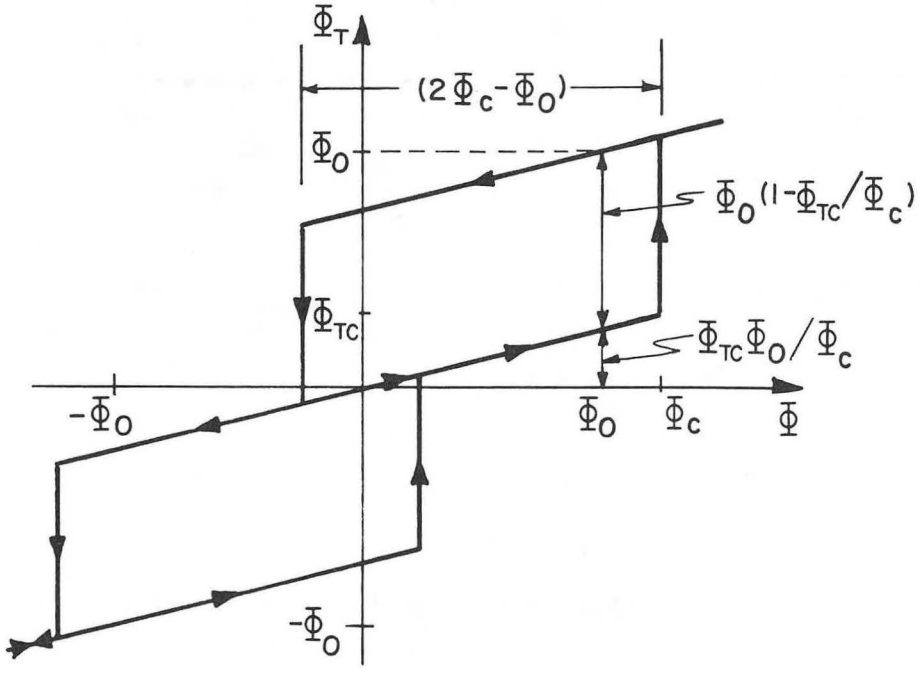

(b)

XBL 766-7132A

Fig. 9

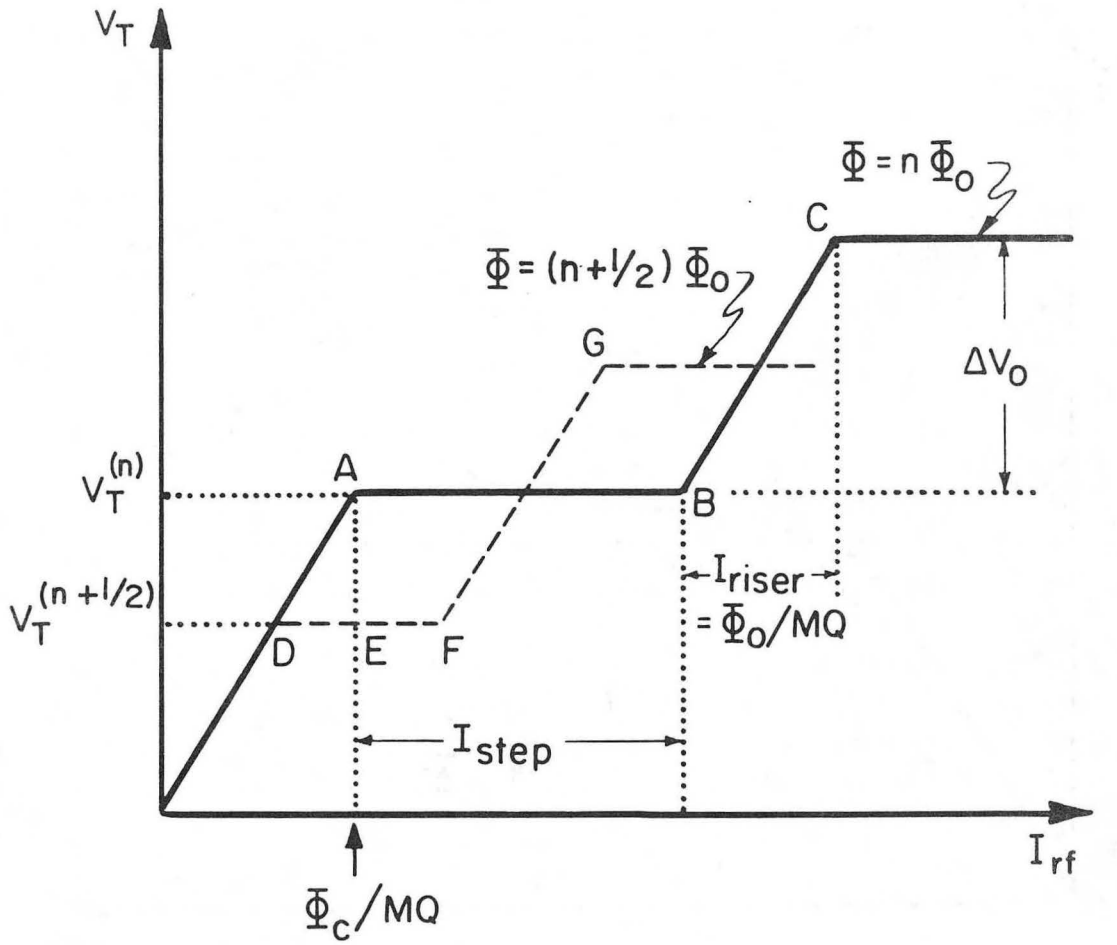

XBL766-7134A

Fig. 10

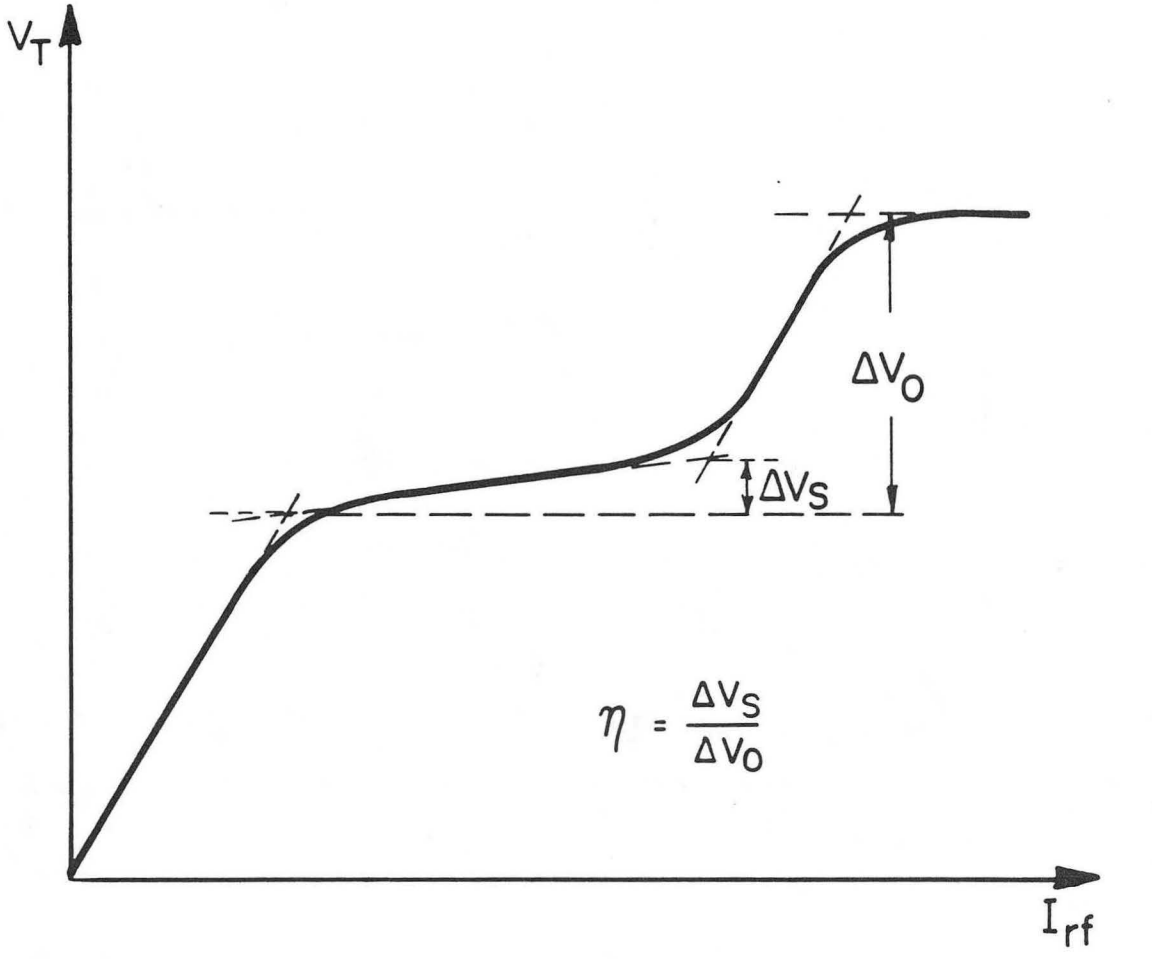
V_T
ΔV_o
ΔV_s
$\eta = \frac{\Delta V_s}{\Delta V_o}$
I_{rf}
XBL766-7135A

Fig. 11

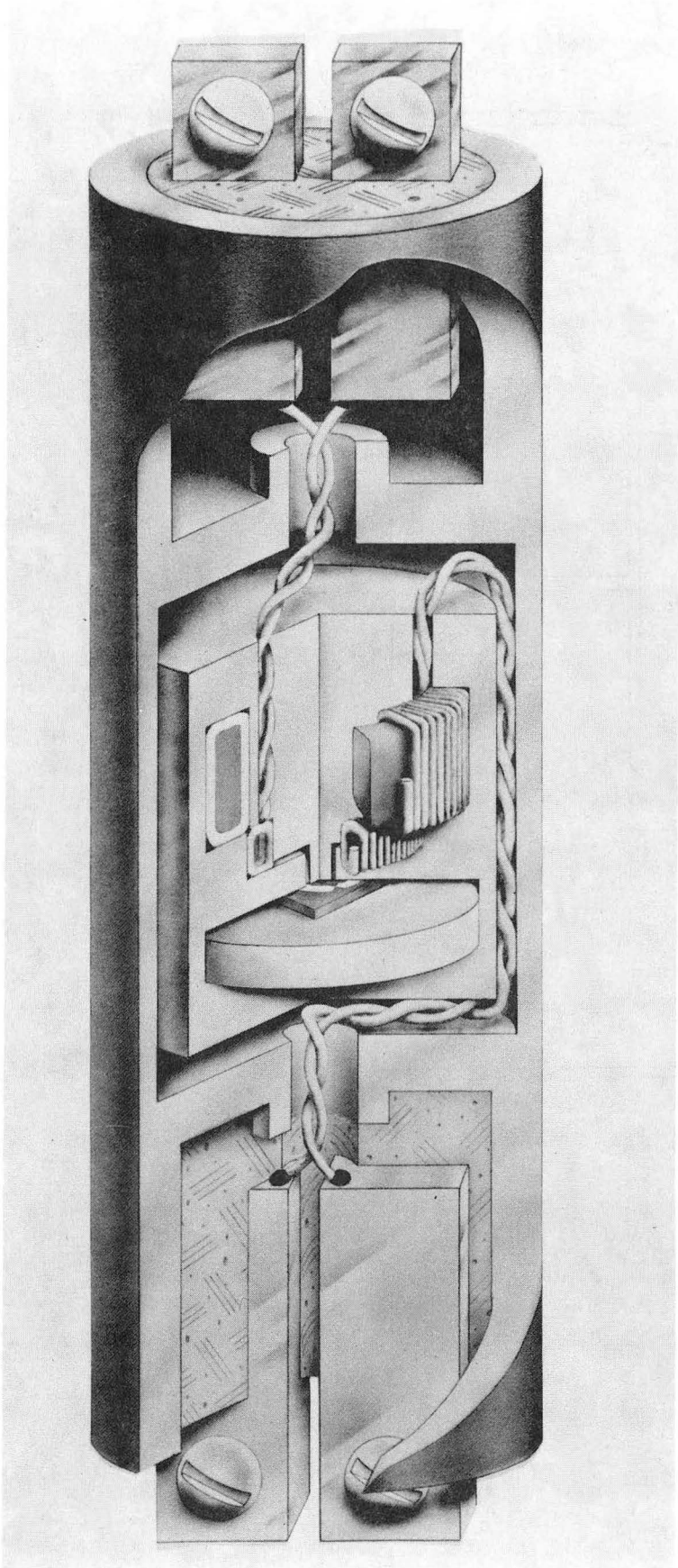

XBB 889-9417

Fig. 12

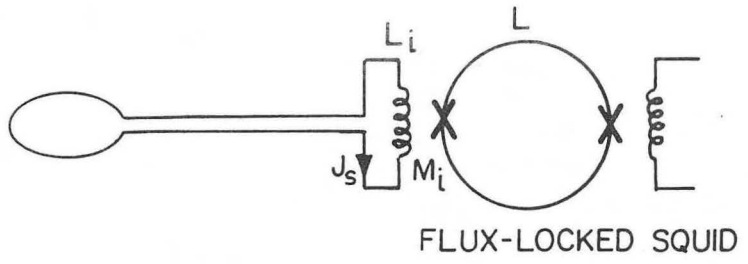

(a)

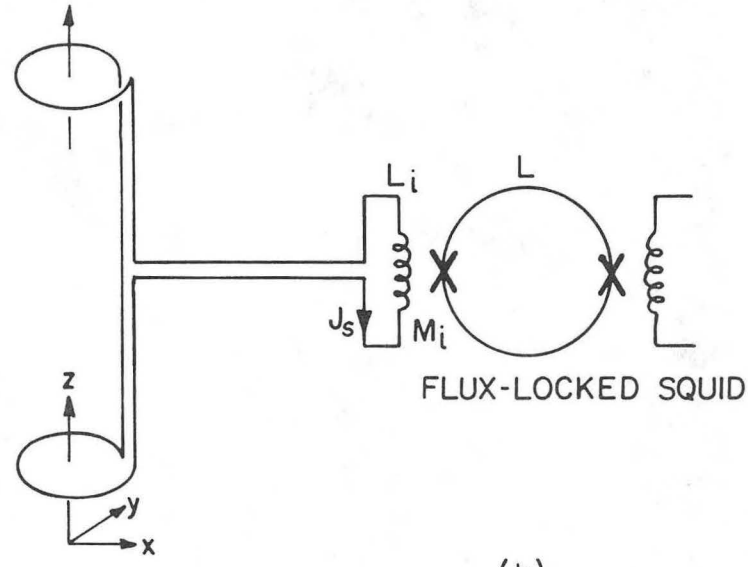

(b)

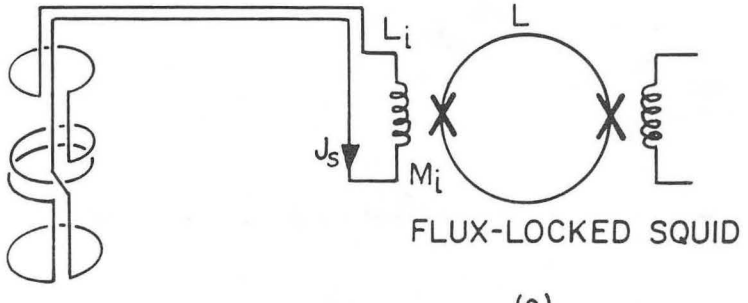

(c)

XBL 766-7138A

Fig. 13

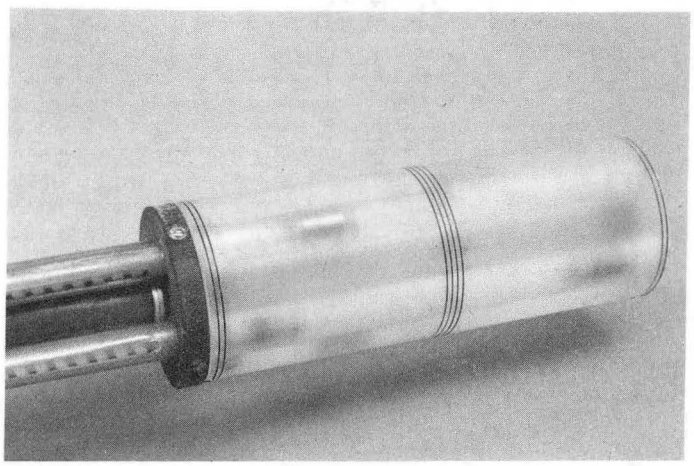

(a) CBB 889-9186

Fig. 14(a)

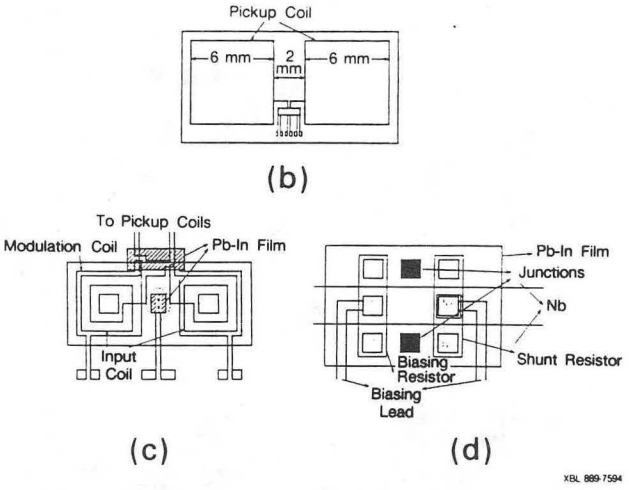
Pickup Coil
6 mm
2 mm
6 mm
(b)
To Pickup Coils
Modulation Coil
Pb-In Film
Input Coil
(c)
Pb-In Film
Junctions
Nb
Shunt Resistor
Biasing Resistor
Biasing Lead
(d)
XBL 889-7594

Fig.14(b)-(d)

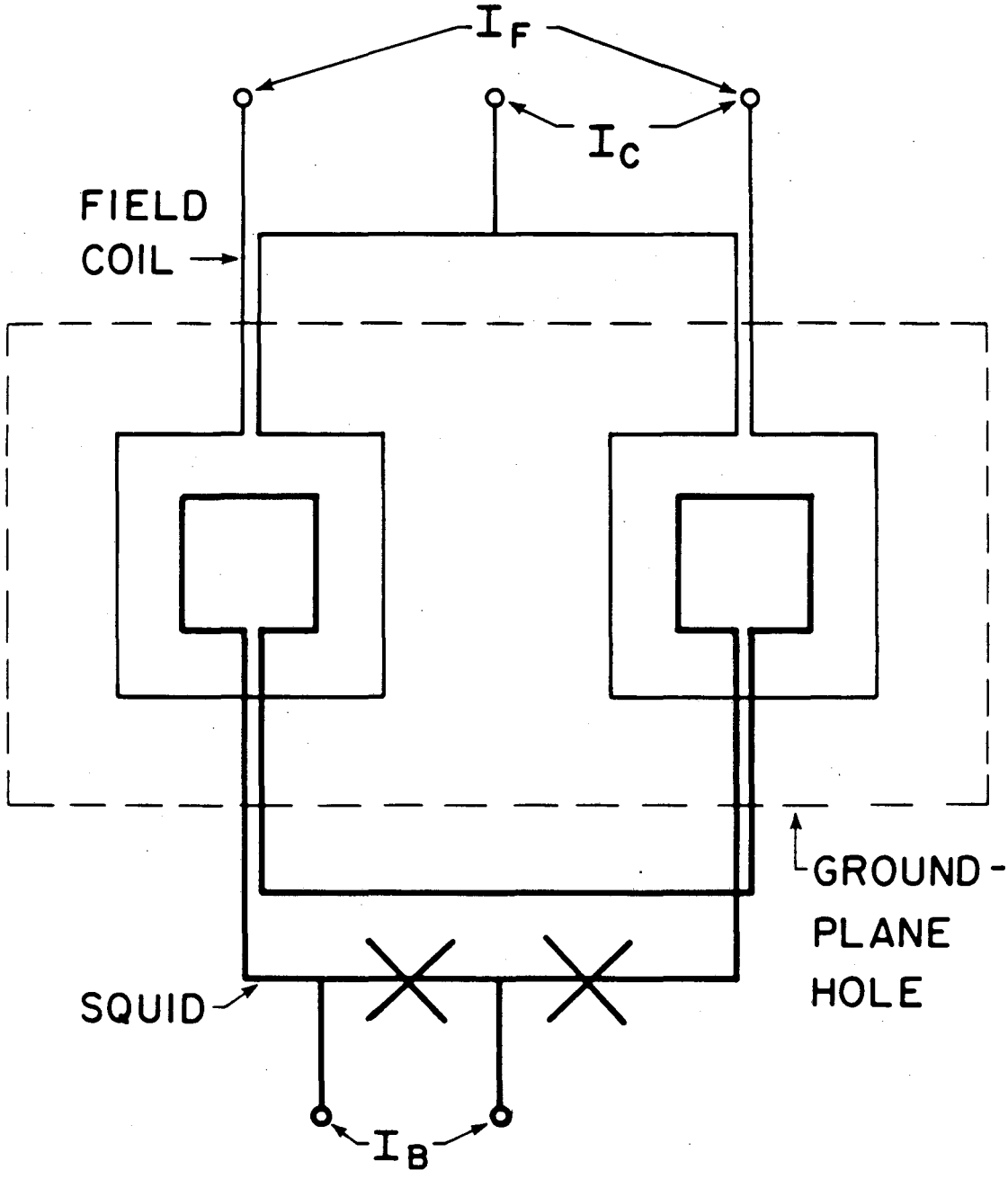

XBL 848-3596

Fig. 15

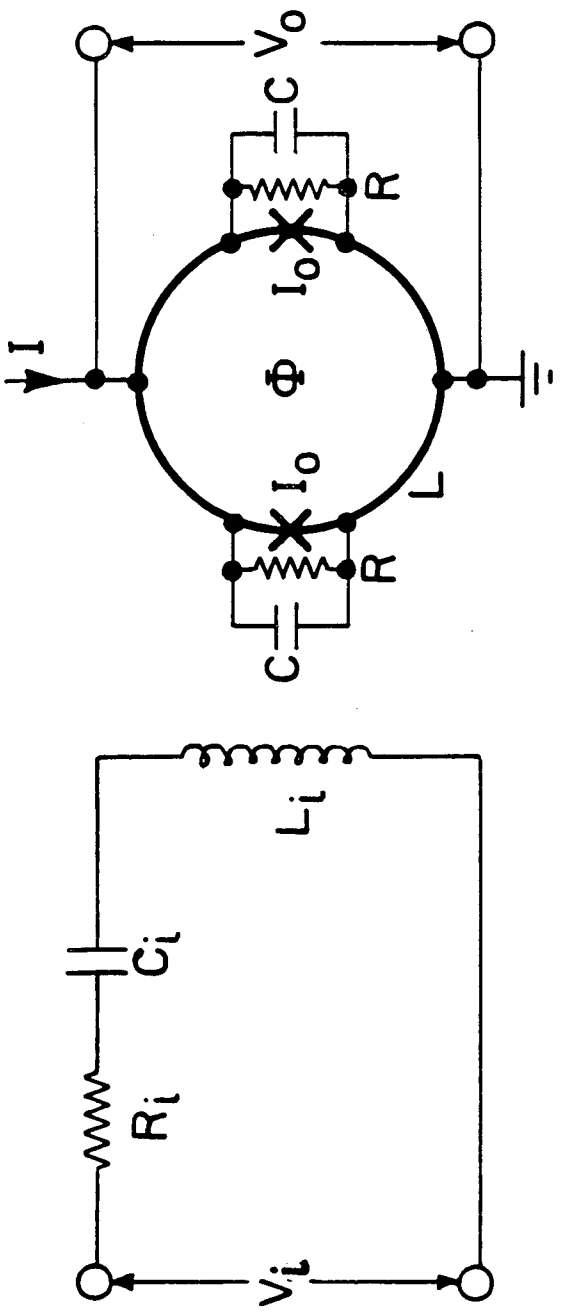

XBL 8010-6148

Fig. 16

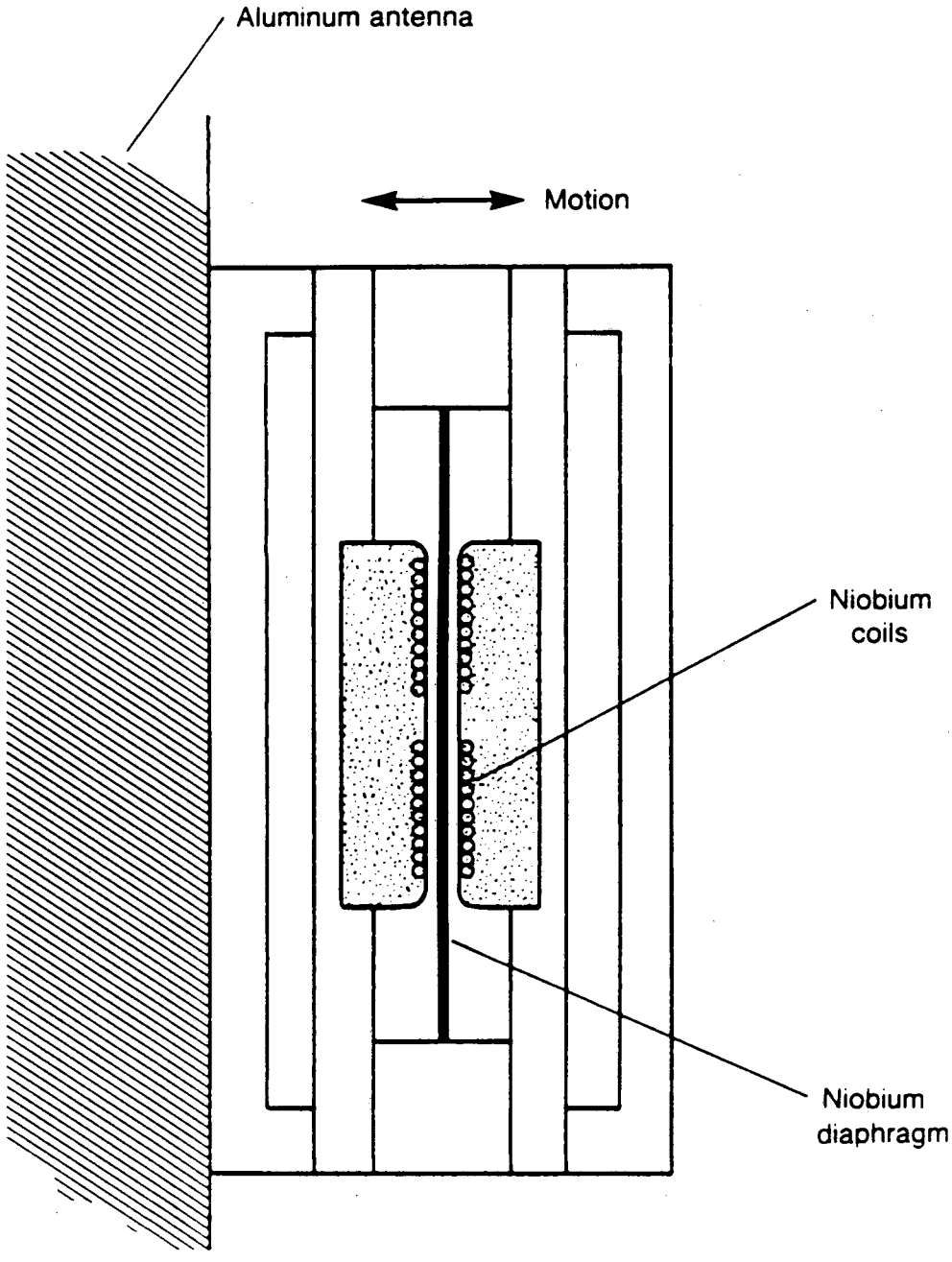

XBL 889-3376

Fig. 17

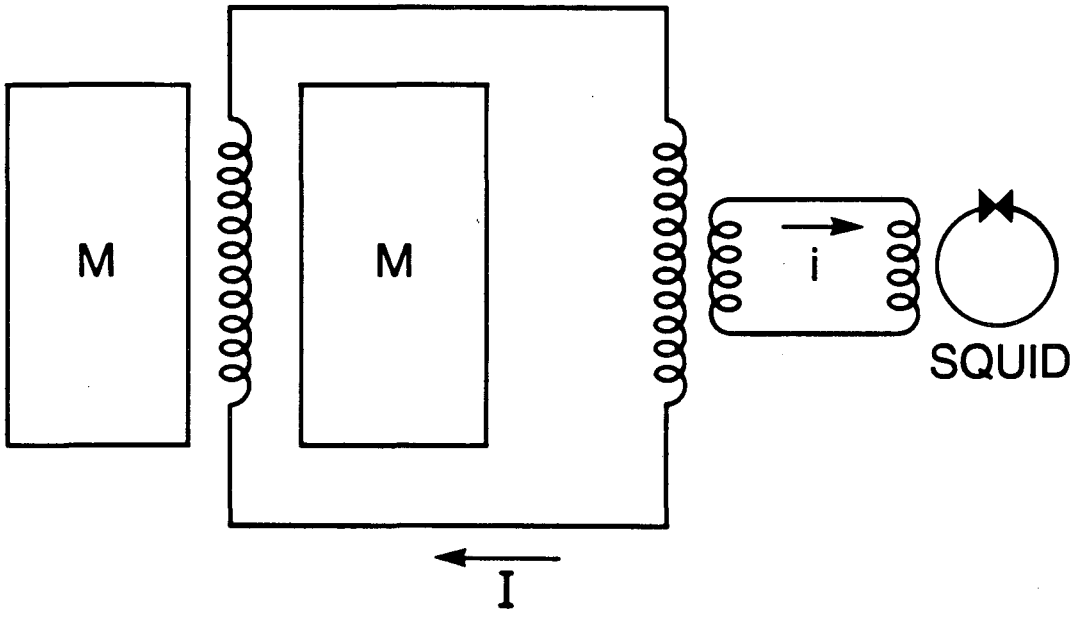

XBL 889-7580

Fig. 18

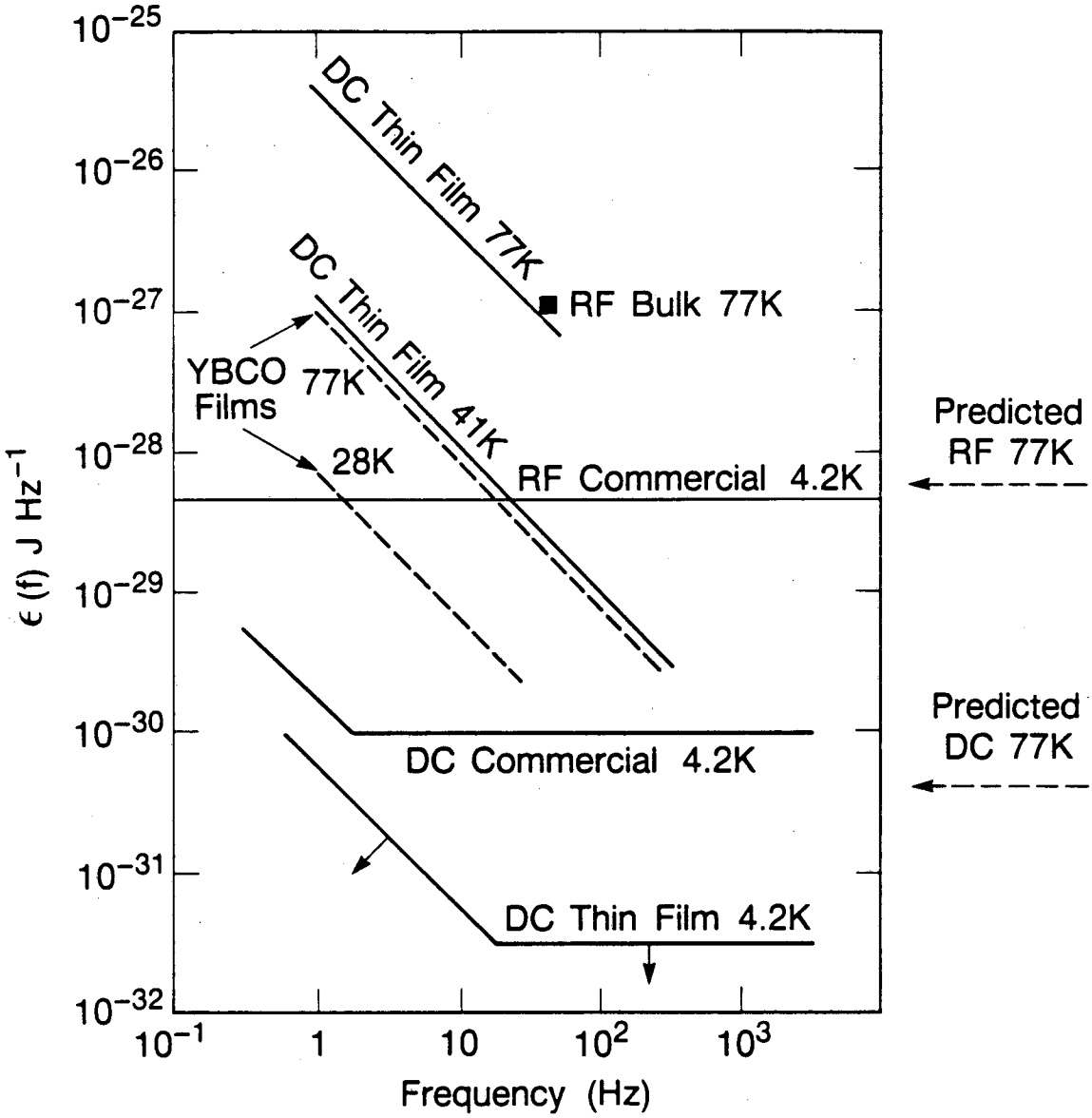

XBL 889-7582

Fig. 19

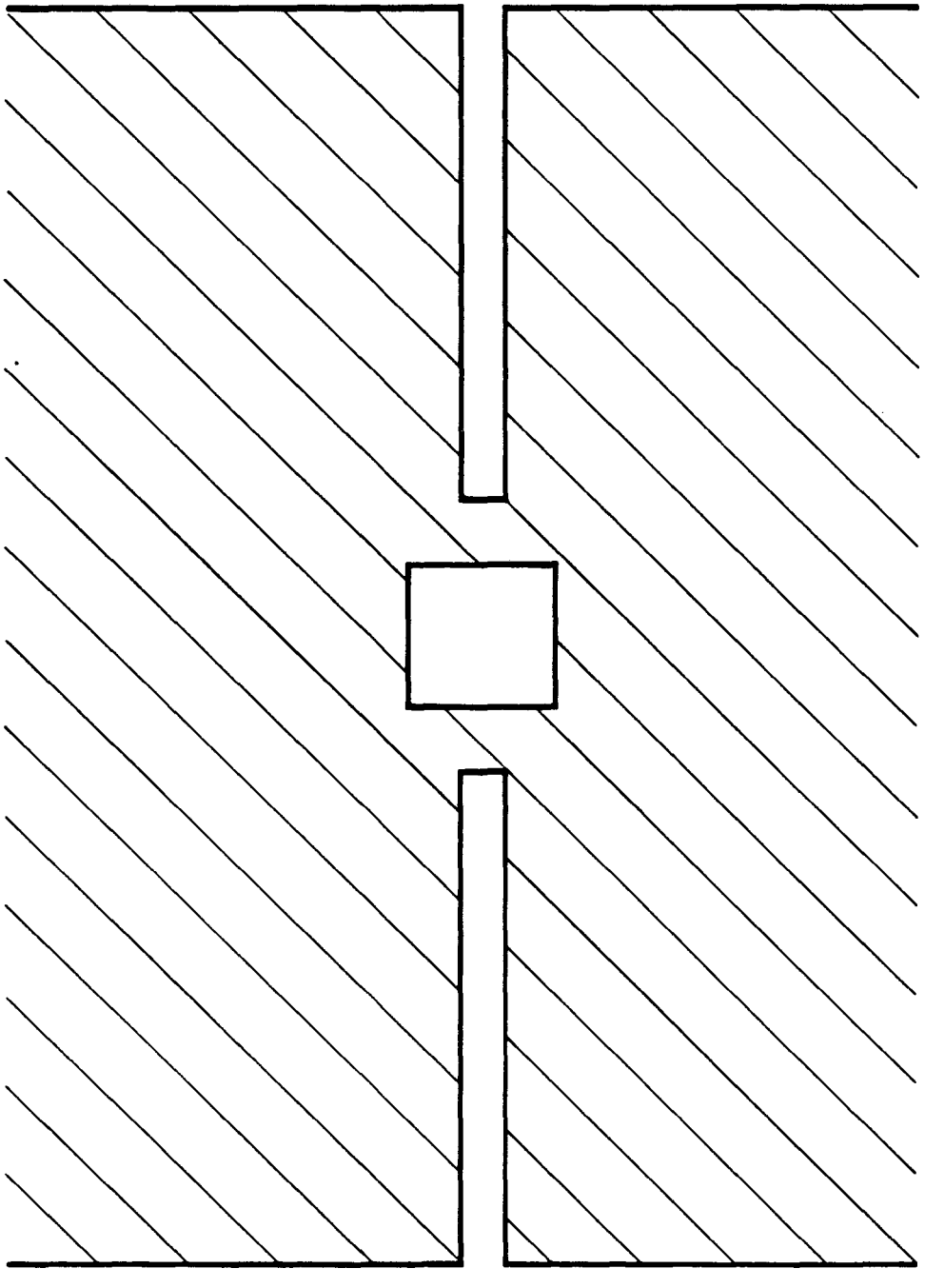

XBL 881-8307

Fig. 20

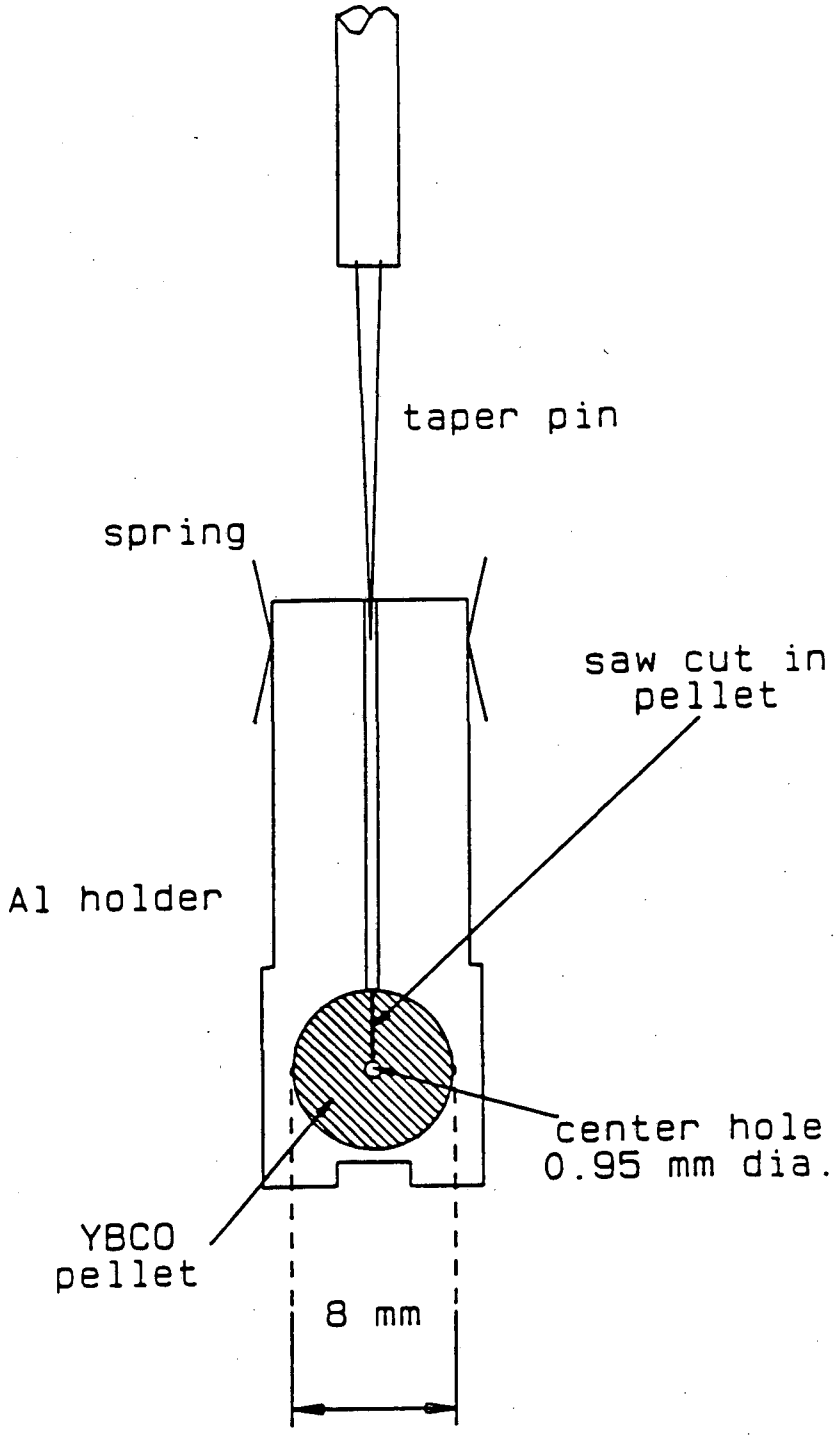

XBL 882-461

Fig. 21

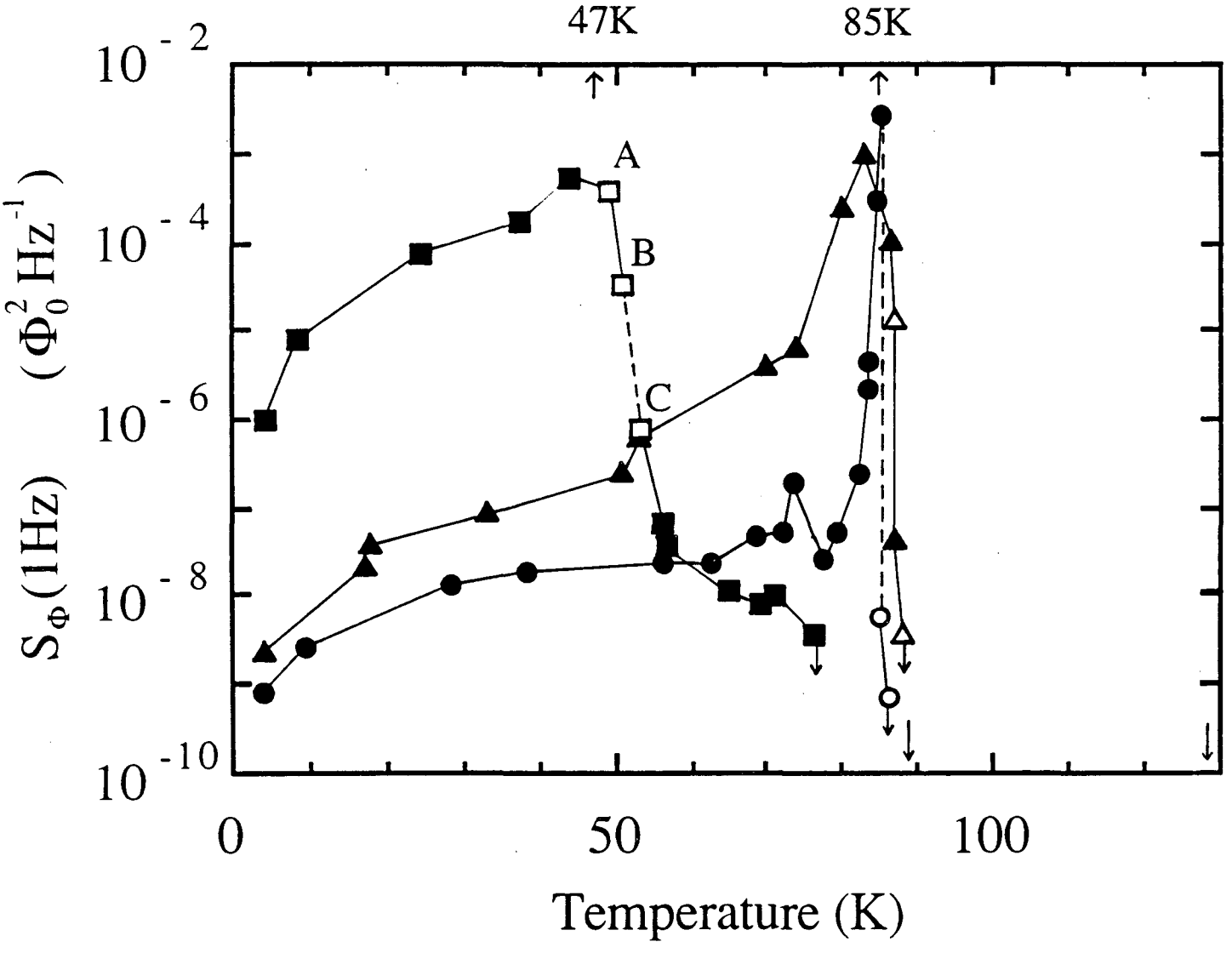

XBL889-3440

Fig. 22

LAWRENCE BERKELEY LABORATORY
TECHNICAL INFORMATION DEPARTMENT
1 CYCLOTRON ROAD
BERKELEY, CALIFORNIA 94720